On the motion of three point vortices in a periodic strip

BY HASSAN AREF AND MARK A. STREMLER
Department of Theoretical and Applied Mechanics
University of Illinois at Urbana-Champaign
Urbana, IL 61801-2935, USA

(Submitted to *J. Fluid Mech.* – June 6, 1995)

Abstract

Motivated by observations of Williamson and Roshko of the wake of an oscillating cylinder with three vortices per cycle, and by the analyses of Rott and Aref of the motion of three vortices with vanishing net circulation on the unbounded plane, the integrable problem of three interacting, periodic vortex rows is solved. The problem is "mapped" onto a problem of advection of a passive particle by a certain set of fixed point vortices. The results of this "mapped" problem are then re-interpreted in terms of the motion of the vortices in the original problem. A rather complicated structure of the solution space emerges with a surprisingly large number of regimes of motion, some of them somewhat counter-intuitive. Representative cases are analyzed in detail, and a general procedure is indicated for all cases. For rational ratios of the vortex circulations all motions are periodic. For irrational ratios this is no longer true. The point vortex results are compared to the aforementioned wake experiments and appear to shed light on the experimental observations. Many additional possibilities for the wake dynamics are suggested by the analysis.

1. Introduction

Several investigators have explored the wake patterns formed by an oscillating cylinder in a uniform stream. In addition to the familiar Kármán vortex street with two vortices per shedding cycle, many complex patterns have been observed, including a mode in which the far-wake region contains three vortices from each shedding cycle. From a large body of literature we mention the studies by Honji & Taneda (1968), Griffin & Ramberg (1974), and Williamson & Roshko (1988), who found that oscillation of a cylinder *normal* to a uniform stream can produce three-vortex patterns. Williamson & Roshko (1988) provide a parameter range over which they found this mode to occur. Griffin & Ramberg (1976), Couder & Basdevant (1986), and Ongoren & Rockwell (1988) also observed the three-vortex pattern, but for a cylinder oscillating *in-line* with the uniform stream.

In analogy to the well known analysis by von Kármán* these observations suggest the following model problem: Consider the (x,y) plane partitioned into an infinite sequence of strips perpendicular to the x-axis. Let the width of each strip be L. Consider a system of three point vortices placed in one of these strips and periodically continued to all the other strips. Thus, each "base" vortex corresponds to an infinite row of identical, uniformly spaced vortices, separated one from the next by a distance L. Since the three vortices are to arise from one cycle of a shedding process, we assume in the model that their circulations sum to zero. (This

*) The question arises as to whether a three-dimensional problem can be accurately (and adequately) represented by a two-dimensional model. In this regard we are on more solid ground than von Kármán, for it is well known that a stationary cylinder can shed vortex filaments obliquely, making three-dimensional effects important. However, in the case of an oscillating cylinder, Koopman (1967) and Griffin, Skop & Koopman (1973) have shown that for sufficiently large amplitudes of oscillation (≥10% of the cylinder diameter) and appropriate Reynolds numbers the wake becomes essentially two-dimensional.

assumption is supported by the observations of Williamson & Roshko, 1988). The problem, then, is to elucidate the motion of this three-vortex problem with the boundary conditions of the periodic strip. As discussed in greater detail below the problem posed is integrable and can, in principle, be reduced to quadratures. The details of the solution, however, are surprisingly complex.

It is not difficult to show that the dynamics of N point vortices in a periodic strip is given by the equations

$$\frac{d\bar{z}_\alpha}{dt} = \frac{1}{2iL}\sum_{\beta\neq\alpha}\Gamma_\beta \cot\left\{\frac{\pi}{L}(z_\alpha - z_\beta)\right\}. \tag{1.1}$$

In these equations the z_α, α=1,...,N, are complex positions of a set of "base vortices", $z_\alpha=x_\alpha+iy_\alpha$. The Γ_β are the circulations of these vortices. The sum is over all base vortices β different from vortex α, the vortex whose velocity is being computed. The overbar on the left hand side indicates complex conjugation. In the limit $L\to\infty$ these equations reduce to the standard point vortex equations on the unbounded plane. The cotangent interaction between base vortices in (1.1) captures the mutual interactions of each base vortex with the periodic images of all the other base vortices. (The contribution to the velocity of a base vortex from its own periodic images vanishes.)

Although the system (1.1) has been discussed in the literature for many years, its power in addressing problems of vortex rows has not always been appreciated and the literature contains several instances of discovery and re-discovery of solutions to these equations. The well known Kármán vortex street arises for N=2 with the condition $\Gamma_1 + \Gamma_2 = 0$. The common translation velocity of the vortices follows immediately from (1.1) specialized to this case. In this paper our objective is to discuss solutions of (1.1) for the case N=3 under the further condition that

$$\Gamma_1 + \Gamma_2 + \Gamma_3 = 0. \tag{1.2}$$

This condition should be met by three vortices produced during one shedding cycle in a wake as in the experiments of Williamson & Roshko (1988). Of course, the perfect spatial periodicity that we are imposing in the model is not entirely realistic. The experimental situation does not have upstream-downstream symmetry. Nor, to be entirely precise, is an exact periodicity downstream of the cylinder to be expected due to the influence of the gradually decaying wake "mean flow". Similar objections can be raised in the case of von Kármán's model of the vortex street. However, the history of the subject amply shows that his consideration of a point vortex model was worthwhile. We feel that similar comments will be made for the N=3 case once the results of the analysis are assimilated.

The problem just outlined has particular theoretical importance in the theory of point vortex dynamics. It has been established that the point vortex equations on the unbounded plane are integrable for N≤3 and *any values* of the circulations (Gröbli 1877; Synge 1949; Novikov

1975; Aref 1979, 1983, 1985; Aref, Rott & Thomann 1992). Integrability comes about due to the existence of certain general integrals of Eqs.(1.1), in particular the *linear impulse,*

$$Q + iP = \sum_{\alpha} \Gamma_\alpha z_\alpha, \tag{1.3}$$

(where Q and P are the real and imaginary parts, respectively), the *angular impulse,*

$$I = \sum_{\alpha} \Gamma_\alpha |z_\alpha|^2, \tag{1.4}$$

and the "Hamiltonian" of the interacting vortices, a quantity related to the kinetic energy of the fluid motion induced by the presence of the vortices. The integrals (1.3) and (1.4) are related to the invariance of the interaction of the vortices under continuous spatial symmetries. Thus, Q is conserved due to translational invariance of the system in the y-direction, P due to translational invariance in the x-direction, and I is conserved due to invariance of interactions under rotation of the coordinates.

On the unbounded plane the solution of the three-vortex problem in the general case (where the sum of the circulations is not zero) is based on the integral (1.4) and the Hamiltonian (see the literature just cited). When the sum of the circulations is not zero, the integral (1.3) can in essence be eliminated by a shift of the origin of coordinates. For the special case of vanishing total circulation, however, the solution is most simply based directly on the invariance of Q and P. Details for this case (on the unbounded plane) have been presented by Rott (1989) and Aref (1989). In particular, it was shown that the problem can be "mapped" onto a problem of advection of a passive particle by three fixed vortices, in much the same way as the Kepler problem in celestial mechanics of two mass points orbiting one another under the influence of Newtonian gravitation can be mapped onto the motion of a single particle in the gravitational field of a fixed point mass. Prof. Rott's suggestion several years ago that the integrable problems of few-vortex systems with zero net circulation would repay more detailed exploration has been an important driving force in our considerations, and has shown itself to be very fruitful.

One might worry that in the periodic strip system only Q would survive as an integral. However, as first remarked by Birkhoff & Fisher (1959), P is also conserved in this case. The integral I, of course, cannot be retained. This opens up the possibility of integrating the problem of three vortices in a strip under the special condition (1.2), since the sum of the circulations appears as the Poisson bracket between Q and P, and when this commutator vanishes, Q and P are integrals in involution. These formal points were demonstrated several years ago (Aref 1985), and unpublished numerical experiments by Blomberg (1984) suggested that the system (1.1) for N=3 is chaotic when condition (1.2) is violated. Thus, the particular case that is relevant to the experiments is also – fortunately – precisely the integrable one. Initially, we thought that the solution for this case would be a straightforward extension of the

work reported in Rott (1989) and Aref (1989). As we shall see, this is not at all the case. Depending on the actual values of the strengths, the solution to this integrable three-body problem can become very complicated indeed. Some motions that arise appear to us almost counter-intuitive. However, as we shall suggest towards the end of this paper, counterparts of these motions, which play a significant role in the overall dynamics of the problem, appear to arise in the experiments of Williamson & Roshko (1988).

It may be appropriate to mention that the special case of vanishing circulation also plays an important role in the case of *four* point vortices which is, in general, a nonintegrable system. Eckhardt & Aref (1988) noted that on the unbounded plane the case N=4, with vanishing total circulation and the additional constraint that Q=P=0, is integrable. A detailed analysis was given by Eckhardt (1989) with two important postscripts by Rott (1990, 1994). In fact, this case "maps" onto a three-particle problem that is similar to the general three-vortex problem on the unbounded plane, an observation that we hope to elaborate on elsewhere. In the periodic strip case the modes observed by Williamson & Roshko (1988), in which there are four vortices per cycle, presumably correspond to non-integrable point vortex systems, and would appear to be even more complicated than the three-vortex cases treated in this paper.

We remark that the methods pursued here may be extended to the case of three point vortices in a general periodic domain in the plane (in which case the periodicity assures us that the sum of the circulations is zero). We intend to report on that case, which is relevant to the study of homogeneous, isotropic two-dimensional turbulence, in a separate paper.

2. Solution method – preliminary considerations

In order to motivate later considerations, we initially follow the solution path from Aref (1989). We shall see soon enough where it fails us. From (1.2) and (1.3) we find

$$\Gamma_2 (z_1 - z_2) + \Gamma_3 (z_1 - z_3) = -(Q + iP) \tag{2.1a}$$

$$\Gamma_1 (z_1 - z_2) - \Gamma_3 (z_2 - z_3) = Q + iP \tag{2.1b}$$

so that simple linear relations allow all three vortex separations to be expressed in terms of one, which we take as

$$z_1 - z_2 = \zeta. \tag{2.2}$$

Thus,

$$\Gamma_3 (z_1 - z_3) = -(Q + iP) - \Gamma_2 \zeta, \tag{2.2a}$$

$$\Gamma_3 (z_2 - z_3) = -(Q + iP) + \Gamma_1 \zeta. \tag{2.2b}$$

Without loss of generality we may assume that the labels of the vortices have been chosen such that $\Gamma_1 \geq \Gamma_2 > 0$, $\Gamma_3 < 0$, since two of the vortices must always have the same sign and the case of two negative vortices follows easily from the case of two positive vortices. We set

$$\gamma = \frac{\Gamma_2}{\Gamma_3} + \frac{1}{2}, \tag{2.3a}$$

and then have

$$\frac{\Gamma_1}{\Gamma_3} = -\gamma - \frac{1}{2}, \tag{2.3b}$$

$$\frac{\Gamma_1}{\Gamma_2} = \frac{1+2\gamma}{1-2\gamma}. \tag{2.3c}$$

It follows from these relations that we cover the necessary range of parameters by allowing γ to vary between 0 and $\frac{1}{2}$.

From the equations of motion,

$$\frac{d\bar{z}_1}{dt} = -i\left\{\Gamma_2 C(z_1 - z_2) + \Gamma_3 C(z_1 - z_3)\right\}, \tag{2.4a}$$

$$\frac{d\bar{z}_2}{dt} = -i\left\{\Gamma_1 C(z_2 - z_1) + \Gamma_3 C(z_2 - z_3)\right\}, \tag{2.4b}$$

$$\frac{d\bar{z}_3}{dt} = -i\left\{\Gamma_1 C(z_3 - z_1) + \Gamma_2 C(z_3 - z_2)\right\}, \tag{2.4c}$$

where the abbreviation:

$$C(x) = \frac{\cot\left\{\frac{\pi}{L}x\right\}}{2L}, \tag{2.4d}$$

has been used, we obtain an equation for ζ:

$$\frac{d\bar{\zeta}}{dt} = i\Gamma_3\left[C(\zeta) + C\left\{X - \left(\gamma + \tfrac{1}{2}\right)\zeta\right\} - C\left\{X - \left(\gamma - \tfrac{1}{2}\right)\zeta\right\}\right], \tag{2.5}$$

where

$$X = -\frac{Q + iP}{\Gamma_3}. \tag{2.5'}$$

And here the main difference between this case and the case of the unbounded plane is apparent. For the unbounded plane we had equations of the form (2.4), and thus (2.5), but the function C in that case was simply $C(x) = \frac{1}{2\pi}x^{-1}$. Hence, quantities such as $C\left\{X - \left(\gamma \pm \frac{1}{2}\right)\zeta\right\}$

could be rewritten in the form $AC(\zeta - B)$ with suitably chosen constants A and B. This allowed the right hand side of the counterpart of Eq.(2.5) (see Eq.(A6) of Aref, 1989) to be interpreted immediately as an advection problem for a passive particle in the field of three fixed vortices.

For the case at hand such an interpretation is more elusive. In the next subsection we consider the special case $\gamma=0$ ($\Gamma_1 = \Gamma_2$). Based on insight derived from that case we present in §4 a general solution method for *any rational value* of γ. An interpretation of the motion in terms of an advection problem in a (wider) periodic strip is possible in this case. Depending on the width of the strip and the number of fixed vortices in it that advection problem may become quite complicated. Representative examples are given in §5, concentrating on the case $\Gamma_1:\Gamma_2:\Gamma_3 = 2:1:(-3)$, which seems to capture the essential regimes of motion that we have observed for other rational values of γ, but that do not arise for $\gamma=0$. In §6 we return to the results of Williamson & Roshko (1988) and argue that, indeed, a counterpart of one of the dominant modes of motion found in the analysis of §§4-5 appears to occur in the experiments. Finally, in §7 we show how the reduction to an advection problem may be obtained for an arbitrary real value of γ. The advection problem now does not "fit" into a periodic strip but involves three infinite rows of fixed vortices. We also discuss the issue of "convergence" of a series of periodic advection problems corresponding to rational approximants of an irrational γ to the infinite row case corresponding to γ itself.

3. The special case $\gamma = 0$ ($\Gamma_1 = \Gamma_2$)

The equation to be solved in this case is

$$\frac{d\bar{\zeta}}{dt} = i\Gamma_3\left[C(\zeta) + C\left\{X - \tfrac{1}{2}\zeta\right\} - C\left\{X + \tfrac{1}{2}\zeta\right\}\right]. \tag{3.1}$$

In order to interpret this as an advection problem by fixed vortices (in a periodic strip) we note the identity

$$2\cot\left(\frac{\pi}{L}\zeta\right) = \cot\left\{\frac{\pi}{2L}\zeta\right\} + \cot\left\{\frac{\pi}{2L}(\zeta - L)\right\}. \tag{3.2}$$

Thus, (3.1) may be rewritten

$$\frac{d\bar{\zeta}}{dt} = i\Gamma_3\left[c(\zeta) + c(\zeta - L) - 2c(\zeta - 2X) - 2c(\zeta + 2X)\right], \tag{3.3}$$

where

$$c(x) = \frac{\cot\left\{\frac{\pi}{2L}x\right\}}{4L}. \tag{3.3'}$$

This equation has an immediate interpretation as an advection problem for a passive particle in

the field of *four* fixed vortices, two of strength $-\Gamma_3$, two of strength $2\Gamma_3$, in a periodic strip of width 2L. The two vortices of strength $-\Gamma_3$ are located at z=0 and z=L. The two vortices of strength $2\Gamma_3$ are located at $\pm 2X$ (mod 2L). Note that the strengths of the advecting vortices do not sum to zero.

A particularly simple case arises if X=0. Then there are just two advecting vortices, one of strength $3\Gamma_3$ at z=0 and one of strength $-\Gamma_3$ at z=L in the strip of width 2L. The pattern of particle paths (or, equivalently, streamlines) in the steady flow produced by these fixed vortices is shown in Figure 3.1. There are four regimes of motion, labelled I, II, III and IV in Figure 3.1. Here and subsequently, regimes of motion are designated by Roman numerals, motions along separatrices by lower case Greek letters, and stagnation (saddle) points by upper case English letters. The motion is bounded, in the sense that $|\zeta|$ is bounded, in regimes III and IV, unbounded in regimes I and II. According to (2.2) this means that the corresponding trajectories of the three vortices in "real space" are such that vortices 1 and 2 stay together in regimes III and IV, whereas they separate in regimes I and II. According to (2.2a) and (2.2b) when vortices 1 and 2 separate, all three vortices will separate, i.e., although they start in the same periodic strip, they will over time migrate farther and farther away so that these base vortices are eventually separated by many strips. There are, of course, periodic images in each strip, but the effect remains that considerable interchange or "mixing" occurs along the rows in this case compared to cases when the base vortices remain within one or two strips of each other for all time. The top three panels in Fig.3.2 display typical trajectories of the base vortices for each of the four regimes in Fig.3.1 according to the labels indicated. Note that in this case the condition X=0 means $z_3 - z_1 = -(z_3 - z_2)$, so (2.4c) shows that z_3 is constant, i.e., vortex 3 remains stationary. The conventions used in Fig.3.2 (and later in other trajectory plots) are that the original base vortices are indicated by solid circles. Their initial positions are given by the numbers 1, 2 and 3; the final positions by 1', 2' and 3' (when it moves). Motion in regime II looks exactly like motion in regime I except that the numbering of vortices 1 and 2 is interchanged. The bottom two panels of Fig.3.2 correspond to the separatrices α, β and γ, δ in Fig.3.1, respectively.

The very simple picture that emerges for X=0 is immediately complicated when $X \neq 0$. Figure 3.3, for example, shows the result of the same construction for X=(1+i)/8. Now we encounter all four advecting vortices (in a strip of width 2L), and so to the simple picture of regimes I-IV in Fig.3.1 we must add regimes V, VI and VII to accommodate the two additional vortices. The dividing streamlines of the advection problem are as shown in Fig.3.3. It is clear that in the advection problem all trajectories are closed in the sense that they either close on themselves or on their periodic image in the next strip of width 2L. Hence, all real-space motions of vortices are periodic, and the initial configuration re-assembles itself after some time, possibly modulo periodic strip, i.e., the new configuration may employ the periodic image of one or more base vortices. Figure 3.4 provides sample trajectories of motions in the various regimes of Fig.3.3 as indicated by the labels. The conventions used in Fig.3.4 are again that the original base vortices are indicated by solid circles. Their initial positions are given by the numbers 1, 2 and 3; the final positions by 1', 2', 3'. In some cases (e.g., I, II and α, β) the

motion of periodic images is essential to understanding how the initial configuration re-emerges after one period of the motion. In these cases the required periodic images and their initial and final positions are indicated by open circles and numbering 2", 3" for the final positions. The trajectories of periodic images are given by lighter lines than the trajectories of the base vortex trio.

Note that in regime I (II) the re-assembly of the initial configuration arises by vortex 1 (2) "teaming up" with periodic images of vortices 2 (1) and 3. In the other regimes the vortices from one strip "travel together" and re-assemble the initial configuration at some shifted position. The four bottom panels in Fig.3.4 show separatrix motions as labelled in Fig.3.3. It can be seen here that the separatrices really tell much of the story in the sense that the motion in any one of the regimes resembles the motion along the separatrices bounding that regime. For example, the motion in the panel labelled III in Fig.3.4 is a "mixture" of the separatrix motions labelled γ, δ and ε, ζ, as would be expected from Fig.3.3. Similarly, the motion in regime I (II) follows quite closely the motion corresponding to the separatrix α (β). This idea, that the general motion can be understood on the basis of the separatrix motions in the advection problem, will be illustrated further as we proceed. Note, however, that the motions within regimes are strictly periodic, whereas the separatrix motions begin and end infinitesimally close to an unstable steady state. Hence, the extent (in real space) of a separatrix motion as displayed in our figures is somewhat arbitrary, since it can be continued "forever" both before and after the segment shown, whereas the trajectory plots within regimes are true single-period motions.

We may emphasize that the saddle points at the end of each separatrix correspond to steadily translating "vortex streets" (with three vortices per period). Because of the reduction to an advection problem, it is clear that only saddle points can appear away from the advecting vortices. Thus, these diagrams also show immediately that the vortex streets in question cannot be stable.

4. Solution method for rational γ

We may base a general approach for the case of rational γ on a generalization of Eq.(3.2). Let us consider a periodic row of identical vortices of strength Γ with spacing L. Assume coordinates are chosen such that the vortices are at x=0, L, 2L, ..., etc. Let us now calculate the induced velocity from this row of vortices on an advected particle at z. First, view the row as a single vortex placed in a strip of width L repeated infinitely in both directions. Then the (complex conjugate of the) velocity in question is simply $(\Gamma/2Li)\cot(\pi z/L)$. Next, view the row as consisting of N identical vortices placed at x=0, L, 2L, ..., (N–1)L in a periodic strip of width NL. Then the velocity is given as a sum of N cot terms. Equating the two expressions we have

$$\frac{\Gamma}{2Li}\cot\left(\frac{\pi}{L}z\right) = \frac{\Gamma}{2NLi}\sum_{n=0}^{N-1}\cot\left\{\frac{\pi}{NL}(z-nL)\right\}, \tag{4.1}$$

or

$$\cot\left(\frac{\pi}{L}z\right) = \frac{1}{N}\sum_{n=0}^{N-1}\cot\left\{\frac{\pi}{NL}(z-nL)\right\}. \tag{4.1'}$$

Introducing the notation

$$c_r(x) = \frac{\cot\left(\frac{\pi}{rL}x\right)}{2rL}, \tag{4.2}$$

(such that C(x) in (2.4d) corresponds to r=1 and c(x) in (3.3') corresponds to r=2) we may write this as:

$$c_1(x) = \sum_{n=0}^{N-1} c_N(z-nL). \tag{4.3}$$

Note also that

$$rc_r(rx) = c_1(x). \tag{4.4}$$

We now return to Eq.(2.5) and assume that γ is a rational number written in lowest terms as p/q, where p and q are integers with q>2p (since $\gamma<\frac{1}{2}$). Using (4.3) and (4.4) we rewrite the second term on the right hand side of (2.5) as follows:

$$C\left\{X-\left(\gamma+\tfrac{1}{2}\right)\zeta\right\} = -c_1\left(\frac{q+2p}{2q}\zeta - X\right) = -\sum_{n=0}^{q+2p-1} c_{q+2p}\left(\frac{q+2p}{2q}\zeta - X - nL\right) =$$
$$\frac{-1}{q+2p}\sum_{n=0}^{q+2p-1} c_1\left(\frac{\zeta}{2q} - \frac{X+nL}{q+2p}\right) = \frac{-2q}{q+2p}\sum_{n=0}^{q+2p-1} c_{2q}\left\{\zeta - \frac{2q(X+nL)}{q+2p}\right\}. \tag{4.5a}$$

Similarly,

$$C\left\{X-\left(\gamma-\tfrac{1}{2}\right)\zeta\right\} = \frac{2q}{q-2p}\sum_{n=0}^{q-2p-1} c_{2q}\left\{\zeta + \frac{2q(X-nL)}{q-2p}\right\}; \tag{4.5b}$$

$$C(\zeta) = \sum_{n=0}^{2q-1} c_{2q}(\zeta - nL). \tag{4.5c}$$

Thus, all three terms on the right hand side of (2.5) have been rewritten in terms of velocities induced by a system of fixed vortices of various strengths in a periodic strip of width 2qL. The total number of fixed vortices is q + 2p + (q – 2p) + 2q = 4q. The differential equation for ζ, which now reads,

$$\frac{d\bar{\zeta}}{dt} = i\,\Gamma_3 \Big[\sum_{n=0}^{2q-1} c_{2q}(\zeta - nL) - \frac{2q}{q+2p} \sum_{n=0}^{q+2p-1} c_{2q}\Big\{\zeta - \frac{2q(X+nL)}{q+2p}\Big\} - \frac{2q}{q-2p} \sum_{n=0}^{q-2p-1} c_{2q}\Big\{\zeta + \frac{2q(X-nL)}{q-2p}\Big\}\Big] \tag{4.6}$$

may be interpreted as a problem of passive advection of a particle in the velocity field produced by these fixed vortices. The special case considered in §3 corresponds to q=1 (and p=0).

For a given $\gamma = p/q$ we are thus instructed by (4.6) to consider the advection of a particle by a system of fixed vortices in a periodic strip of width 2qL. There are three families of vortices. At the 2q locations 0, L, ..., (2q–1)L we find identical vortices of circulation $-\Gamma_3$. The locations of the two other families of vortices depend on the value of the impulse in the original problem, here represented by the quantity X. The q+2p vortices located at $2q(X+nL)/(q+2p) = -(\Gamma_3/\Gamma_1)(X+nL)$, n = 1,..., q+2p–1 all have circulation $2q\Gamma_3/(q+2p) = -\Gamma_3^2/\Gamma_1$; the q–2p vortices at $2q(-X+nL)/(q-2p) = -(\Gamma_3/\Gamma_2)(-X+nL)$, n = 1,..., q – 2p – 1 all have circulation $2q\Gamma_3/(q-2p) = -\Gamma_3^2/\Gamma_2$. Note that although the sum of the original three vortex circulations vanishes, the net strength of the fixed vortices in the advection problem for ζ is $2q\Gamma_3$ ($\neq 0$). When X is real all three families of vortices are situated on the real axis, and depending on the values of p and q, vortices from the different families may coincide (in which case a single vortex is placed with a circulation equal to the sum of the circulations of the coinciding vortices). The streamline pattern in the advection problem tends to simplify, sometimes dramatically, in these cases. When X has a non-vanishing imaginary part, the three families of vortices are always distinct, one family remains on the real axis, the second will be situated above it and the third below it. We shall see later that the topology of the streamlines governing the advection problem can simplify for certain values of the real part of X. Concerning the imaginary part it appears that the only important distinction is whether it is finite or zero.

The motion of a passively advected particle in the flow field induced by these three rows of fixed vortices can be used, via Eqs.(2.2), to construct and classify the trajectories of the original three vortices in the periodic strip. For brevity and clarity we shall refer to the trajectories of the original vortices as the vortex motion in "real space". We shall refer to the advection problem as the motion in "phase space".

We have stressed the notion of "base vortices" from which an entire row may be constructed by periodic continuation. However, the dynamic problem is invariant to a shift by an integral number of periods within the row of which a vortex is considered the "base", i.e., simultaneous shifts of z_1, z_2, and z_3 by integral multiples of L in the original setup lead to the same problem. In terms of the quantity X, Eq.(2.5'), this means that changes in its real part by $-r(\gamma + \frac{1}{2}) + s(\gamma - \frac{1}{2}) + t$, where r, s, and t are integers, lead to the same problem. The smallest positive value that this expression can assume is $\frac{1}{2} - \gamma$. Hence, it is only necessary to vary the real part of X between 0 and $\frac{1}{2} - \gamma$.

In general we expect the "phase space" to be a periodic strip of width 2qL. From the considerations just given we may, however, derive sharper results: Without loss of generality let t=0 so that base vortex 1 is shifted by rL, base vortex 2 by sL. This changes ζ by (r–s)L. In order to be considering an equivalent problem we must assure that X is not changed, i.e., r and s must satisfy $r(\gamma+\frac{1}{2}) = s(\gamma-\frac{1}{2})$. With $\gamma = p/q$ this means $2p(s-r) = q(s+r)$. We are only interested in q>2. Consider first the case where q is odd. Since p and q are relatively prime, this relation tells us that s + r must be a multiple of p and s – r must be a multiple of q, i.e., there must exist an integer k such that s–r= kq, s + r = 2kp. Solving for r and s we have $2s = k(2p + q)$, $2r = k(2p - q)$. Since q is odd, it follows from these that k must be even. The smallest shift in ζ that leads to an equivalent problem thus occurs for k=2, and is 2qL. Thus, the "phase space" will be periodic with period 2qL for odd q and we should not expect a shorter period. For even q the situation is different. We set q = 2u and note that p must now be odd. The equation $2p(s - r) = q(s + r)$ becomes $p(s - r) = u(s + r)$, where u and p are relatively prime. There then exists a k such that $s - r = ku$, $s + r = kp$, and $2s = k(p + u)$, $2r = k(p - u)$. Now, if u is odd, p + u is even, and k=1 gives the smallest value of s – r, viz (q/2)L. On the other hand, if u is even, k must also be even, the smallest value of s – r occurs for k=2, and is qL. Thus, for even q the "phase space" will already be periodic with period qL if q is divisible by 4, and with period (q/2)L if q is not divisible by 4. The latter period is four times shorter than the general result 2qL would have led us to believe. The case (p,q) = (1,6), corresponding to circulations $\Gamma_1:\Gamma_2:\Gamma_3 = 2:1:(-3)$, is the simplest example of a "phase space" with such a shorter period. This case will be studied in detail in §5.

It is not difficult to verify that the coincidence of ζ with one of the vortices in the "phase space" corresponds to the coincidence of two of the original vortices 1, 2, and 3 in real space (modulo L). For example, if $\zeta = 2q(X + nL)/(q + 2p)$, then $z_2 - z_3 = X - (\gamma+\frac{1}{2})\zeta = -nL$. This is, of course, not allowed. However, it is useful to note that ζ-motion in the vicinity of a phase space vortex in the row with positions $2q(X + nL)/(q + 2p)$ corresponds to real space motion in which vortices 2 and 3 "move as a pair". Similarly, ζ-motion in the vicinity of a phase space vortex in the row with positions nL corresponds to real space motion in which vortices 1 and 2 "move as a pair", and ζ-motion in the vicinity of a vortex in the row with positions $2q(X - nL)/(q - 2p)$ corresponds to real space motion in which vortices 1 and 3 "move as a pair". We should recall that the notion of "moving as a pair" can lead to rather different patterns of motion depending on both the relative sign and magnitude of the circulations of the two vortices in the pair.

5. Representative examples

Among the simplest rational values of γ to consider are (p,q) = (1,3), (1,5) and (2,5) corresponding to the vortex strength ratios $\Gamma_1:\Gamma_2:\Gamma_3 = 5:1:(-6)$; $7:3:(-10)$; and $9:1:(-10)$, respectively. In all these cases q is odd and the phase space periodic strip is of width 2qL. The phase space diagram for the case (p,q) = (1,6), where q is even but not divisible by 4, fits in a strip of width 3L. The corresponding vortex strengths, $\Gamma_1:\Gamma_2:\Gamma_3 = 2:1:(-3)$, probably give the

simplest set to consider after the case γ=0 from §3. On one hand, the phase space diagram for this case reveals regimes of motion that are not present for γ=0. On the other hand, it seems to capture the phase space structures that appear for other rational values of γ that we have explored. Hence, we begin our study of specific examples by an analysis of the motion in the case (p,q) = (1,6), and then briefly show how the regimes of motion found for this case have counterparts in more complex motions corresponding to (p,q) = (1,5) and (2,5). We have considered other examples as well, such as (p,q) = (1,3), (1,7), (2,7), and so on, and we have not found regimes of motion qualitatively different from the examples selected for presentation below.

Figure 5.1 shows phase space streamlines for (p,q) = (1,6), and X= $\frac{1}{12} + i\frac{1}{4}$. All streamlines shown are, in fact, separatrices or "dividing streamlines", i.e., they connect stagnation points of the advection problem in a strip of width 3L. The chosen value of X is "generic" in the sense that the streamline pattern does not display any symmetries that may arise for other, more carefully chosen, values of X. For example, in Fig.5.2a,b we show the more symmetric patterns of phase space streamlines that arise for X = $i\frac{1}{4}$ and X = $\frac{1}{6} + i\frac{1}{4}$, respectively. (In general the values of *Re*(X) that lead to symmetry are 0 and $(\frac{1}{2} - \gamma)/2$, mod $\frac{1}{2} - \gamma$.) In the symmetric cases several of the saddle points are connected by separatrices, whereas in the "generic" case such connections do not occur. Consider, for example, the dipole-like structure in Fig.5.1 with regions labelled IV and VIII, and saddle points labelled D and E. One might at first sight think it is an error that there is not a separatrix curve connecting D to E. However, this kind of connection does not arise, and if one traces the separatrices (which is not entirely simple since several of them are very close), one finds that both D and E are connected up to themselves by two loops, i.e., the pattern of separatrices is topologically like a "figure 8" with D or E at the crossing point. These dipole-like structures around a pair of fixed vortices in this problem are thus quite different from the more familiar connected configurations that arise in such problems as the "atmosphere" of a translating vortex pair. We are certain that the streamline topologies in Fig.5.1 are, in general, of this "disconnected" type, and to verify this we have computed to high accuracy the values of the streamfunction at the two saddle points (such as D and E) on either side of an apparent dipole, and we have found them to differ by a few percent. On the other hand, when a symmetrical situation such as Fig. 5.2a or b does occur, the values of the streamfunction at two apparently connected saddle points agree to all significant digits. The existence of these "disconnected" streamline patterns leads to regimes of motion that reside in very thin strips of phase space (e.g., the regions marked IX, XI, and XII in Fig.5.1) yet are clearly identifiable in the real space dynamics of the vortices. A diagram such as Fig.5.1 thus has as many as 13 distinct regimes of motion! We have labelled these by Roman numerals. In Fig.5.3 we show representative real space vortex trajectories (of the base vortices) corresponding to these various regimes. The richness of some of these motions, all of which are periodic, in particular those associated with the aforementioned "thin strips" in phase space (see, for example, the trajectory plot labelled "XI" in Fig. 5.3) is remarkable.

The general nature of each of the trajectory plots in Fig.5.3 can be understood by reference to Fig.5.1 and use of the formulae (2.2). We have already commented on the nature of real

space trajectories when ζ orbits one of the fixed phase space vortices. Examples are shown in panels III, IV, V, VI, VII, and VIII of Fig.5.3. More interesting, and certainly more pervasive in the phase space plot of Fig. 5.1, are the regimes that pass by several of the fixed vortices. Trajectory examples are shown in panels I, II, IX, X, XI, XII and XIII of Fig.5.3. Both bounded and unbounded motions occur in the sense that the original base vortices stay together or separate indefinitely. Bounded motion occurs in regimes IX, X, XI and XII; unbounded motion in regimes I, II and XIII. Clearly, the number of periodic strips that separate the final and initial positions of the base vortices, and whether the re-emergence of the original pattern involves periodic image vortices or not have significant consequences for such processes as mixing. Some of the trajectories (e.g. XI) are quite complex with the vortices moving through very complicated turns, some of them very sharp. We stress that all motions are periodic, and that the complexity seen in Fig.5.3, e.g., that the vortices travel several periodic strip widths before re-arranging into the original pattern, is all happening in periodic motions. We also stress the appearance and prevalence of motions such as I, II since we believe them to be among the ones observed experimentally, as we discuss in §7.

The separatrix motions that connect different steady state "vortex streets" clearly provide a key to understanding the entire diagram. We have computed the real space motion corresponding to the various separatrices in Fig. 5.1, and these are presented in Fig. 5.4. Knowing the separatrix motions in real space and knowing the phase space it is possible to develop a qualitative picture of any real space motion by "piecing together" the appropriate separatrix motions. Thus, a trajectory such as XI in Fig.5.3 is clearly made up of pieces that resemble separatrices κ and μ, i.e., the two "loops" that share saddle point D in Fig.5.1.

An interesting corollary of all these developments is that *there are no stable steady configurations.* Steady configurations of the three vortices in real space correspond to stagnation points of the advecting flow in phase space. These come in two varieties: there are the locations of the advecting vortices, and there are a number of hyperbolic points in the flow field away from the vortices. There cannot be elliptic points in the flow field since it is a potential flow induced by a fixed set of point vortices. Clearly, the real space state corresponding to any hyperbolic point is not stable, since there exist perturbations that will amplify exponentially. And, as we have already seen, the advecting point vortices correspond to real space states in which two vortices are at the same location, i.e., to unavailable states of infinite energy. Thus, the reduction to an advection problem demonstrates immediately that there can be no steady configurations of the original vortices. This statement goes well beyond linear stability theory. We suggest that this mode of analysis can be applied to the conventional vortex street problem, where all the vortices have circulations of the same magnitude, and thus provide an alternate, geometrical route to the full nonlinear stability analysis of that configuration, which is known to be very demanding analytically (Kochin, Kibel & Roze 1964).

Phase space plots and corresponding trajectories are similar for other cases that we have explored. By way of example Fig. 5.5 shows the ζ-plane phase space for (p,q) = (1,5) and $X = \frac{3}{40} + i\frac{1}{4}$. Regimes similar to those observed in Fig. 5.1 will be seen, although there are more of them. The general nature of trajectories, both in phase space and in real space, is again similar to what we have seen in Fig. 5.1 and 5.3. The general nature of the separatrices is similar as

well. Figure 5.6 shows two separatrices (labelled α and β in Fig.5.5). The case q=5 is interesting because it is the smallest denominator for which two values of the numerator, p, are allowed. Thus, in Fig. 5.7 we show the ζ-plane phase space for (p,q) = (2,5) and $X = \frac{1}{40} + i\frac{1}{4}$. The main difference between Figs.5.5 and 5.7 is that the lower row of advecting vortices contains just one vortex in the latter case but three in the former in accordance with the general theory given in §4. Figure 5.8 shows three real space trajectories of the three vortices corresponding to the separatrices labelled α, β and γ in Fig. 5.7. Again the spatial complexity of the motions and the large number of periodic strips (10) over which these periodic motions extend have already emerged in our discussion of Figs.5.3 and 5.6. The "open dipoles" in the ζ-plane clearly have a major role to play in producing this dynamics.

Since we know the number of poles in a phase space strip, it is possible to use simple ideas from the theory of analytic functions to count the number of saddle points (and hence states of steady translation) for a given rational γ, modulo "accidental" degeneracies due to symmetries. In general, i.e., for a general value of the linear impulse, these vortex streets will translate with different velocities and will not be dynamically connected. There will be no separatrix joining them; i.e., the saddle points in the phase space diagram will be homoclinic rather than heteroclinic. The two separatrices belonging to a given saddle will thus, generically, consist of a "short branch", that loops a nearby vortex, and a "long branch", that crosses the periodic boundary of the strip in the phase space diagram. The "short branch" leads to relatively simple motions in which two vortices "move as a pair". The "long branch" leads to the motions that extend over several strip widths as illustrated in Figs.5.4, 5.6 and 5.8.

Based on explorations of various cases using the methods explained above we believe that the general, qualitative nature of the motion has been elucidated in all cases of rational γ. All motions (except for the separatrix motions) are periodic, and it always appears possible to find motions in which two of the base vortices will become separated by 2q periodic strip widths during one period.

6. The case of irrational γ

In general γ will, of course, be irrational. The procedure given in §4 for rational γ does not immediately generalize and, in fact, seems to suffer a convergence problem if one considers a sequence of rational approximants, p_i/q_i, approaching the irrational γ ever more closely. For each of these the construction in §4 may be worked out. The problem is that the denominators in the series of rationals approximants, i.e., the q_i, may fluctuate considerably, so that one is led to consider successive strips and vortex patterns that do not seem to be related or to be converging to a final result in any simple way.

The results obtained in §4 suggest that the problem to be considered is an advection problem for a passive particle in the field of a system of fixed vortices that belong to one of three infinite "families". First, there should be a set of vortices of circulation $-\Gamma_3$ at regularly spaced locations 0, $\pm$L, ... Second there should be a set of vortices of circulation $\Gamma_3/(\gamma + \frac{1}{2}) = -\Gamma_3^2/\Gamma_1$ located at $(X + nL)/(\gamma + \frac{1}{2})$, n=0, $\pm$1,... Finally, there should be a family of vortices of

circulation $-\Gamma_3/(\gamma - \frac{1}{2}) = -\Gamma_3^2/\Gamma_2$ at $(X + nL)/(\gamma - \frac{1}{2})$, n =0, ±1,... (The reader of Rott (1989) and Aref (1989) will recognize these circulation values!) Whereas for rational γ these three rows are a repeat of a basic pattern in a strip with a width that is a multiple of the given strip width, for irrational γ no such strip exists. The incommensurability of the spacings in the three rows means that an infinite system is required.

The same result is obtained analytically (and this provides a different and maybe even simpler approach to the results in §4) if one works directly with the infinite series describing the mutual vortex interactions rather than summing them in cotangents as we did above. Within each series one has terms of the form $(z_1-(z_2+nL))^{-1}$ to account for the influence of base vortex 2 and its periodic images on base vortex 1. There is an infinite sum on integers n for each such term. Within the sums, assuming convergence is assured, the scalings in (2.2) can now be shifted from denominator to numerator, and there can be absorbed in a rescaling of the vortex strength precisely as in the analysis of three-vortex motion on the unbounded plane (Aref 1989). The end result is exactly as stated in the preceding paragraph.

The phase plane streamline pattern of the infinite system of fixed vortices is quite complex. We have already seen in the case of rational γ that the dipole-like structures around two close vortices of opposite sign usually are not closed. In the case of irrational γ it appears furthermore that, in general, *no two dipoles will be connected.* Hence, there will be an infinity of regimes, and since the return of a phase space trajectory through a periodic boundary is precluded, only the ζ-motions confined to the vicinity of a single vortex will be bounded and periodic. Hence, most of the real space motions will resemble the trajectories in Figs.5.6 and 5.8, but will not be periodic (with or without the assistance of periodic images). Only motions for which the initial configuration has two of the vortices sufficiently close so that they "move as a pair" will display periodicity.

7. Comparison with experiments by Williamson & Roshko

In order to compare the solutions obtained for a point vortex model with experimental results several problems must be addressed. Some of these have been known for many years since the well known stability theory of conventional "two-vortices per period" vortex streets was first proposed by von Kármán (see, for example, Lamb 1932, §156). First, in addition to the mutual interaction of the vortices as captured in the model treated here, a real wake has a "mean flow" that advects the vortices downstream. One might attempt to include that flow by adding the potential flow about a cylinder to the mutual interactions of the vortices, but in the present case the oscillation of the cylinder introduces additional complications. Even ignoring the oscillations, downstream variation of the mean flow implies that the periodic strip width used in the temporal model problem should be variable when the results are translated to the spatial problem. Second, the real wake is semi-infinite rather than doubly infinite as assumed in the point vortex model. Even ignoring the mean flow, or assuming it to be simply a constant advecting velocity, the periodicity assumption can only begin to be valid as one travels some finite distance downstream along the wake. Unfortunately, viscous effects (also ignored) have then had some time to act, and the location, concentration and two-dimensionality of the vortices

in the wake can be called into question. Finally, the precise values of the circulations is typically not known in the experiment, although it is reasonable to assume that the total circulation of all vortices shed during a full cycle is zero. It follows from all these caveats that any comparison of our model results with experiments will be quite qualitative, and while the model results clearly can stand on their own merits, we feel that the modeling attempt to be undertaken in this section does increase the understanding of the experimental observations and suggests new experiments on the wake of an oscillating cylinder.

We decided to attempt a comparison of our model problem solutions with the experimental photographs of Williamson & Roshko (1988). Professors Roshko and Williamson have both kindly sent us original photos so that we might have as clear a record as possible for this task. Figure 7.1 summarizes our attempts at fitting one of our solutions to the experimental photograph appearing as Figure 17(c) in Williamson & Roshko (1988). Panel (a) of Fig. 7.1 simply reproduces the experimental photograph. In panel (b) we have plotted the positions of the vortices as measured from the photograph. The triangles connect those vortices that appear to belong to the same shedding cycle. Panel (c) represents our attempt to reproduce the vortex motions of the experiment using the point vortex model. Here the triangles connect a set of "base vortices", in the sense of the preceding discussion, at different instants of time.

In the previous sections, the model problem dealt only with the motion of point vortices in otherwise quiescent fluid. However, the experimental photo in Fig. 7.1(a) was produced by towing a transversely oscillating cylinder through water, with three vortices being shed for each cycle. We neglect any effect of the cylinder on the potential flow downstream, but to compare with experiment we need our coordinate system to translate with the cylinder. That is, the velocity of a vortex must now be due to its interaction with the other vortices plus an advection by a free-stream velocity equal and opposite to the cylinder translation velocity. Now, in order to produce the appropriate picture, we need to specify the translation velocity of the cylinder, the width of the periodic strip to be used for generating our model solution, the vortex strengths, and the initial vortex locations. We mention how we chose these various parameters: The translation velocity and strip width can be determined from the relevant dimensionless parameters Re and L/D, where the Reynolds number is based on the cylinder's translation velocity U and diameter D, and L is the wavelength of the resulting cylinder motion. Williamson and Roshko (private communication) report D=1 in., Re = 275, and L/D=6.0. The periodic strip width is taken as a fixed length, equal to the horizontal distance that the cylinder travels in one cycle, i.e., 6D. We approximate the vortex strengths by using the empirical relationship $K/U^2 = \Lambda$ (see Birkhoff & Zarantonello, 1957) , where U is the free-stream velocity and K is the product of the shedding frequency and the circulation shed from one side of the cylinder. We take Λ=0.32 (Koopman 1967), which was given for a stationary cylinder, but we use it here, nevertheless, as an approximation. Due to viscous effects one expects that about two-thirds of the circulation shed from one side of the cylinder ends up as the circulation associated with a shed vortex. The bottom-most vortex in each triangle (the only vortex shed from the bottom of the cylinder in one cycle) is thus assigned a positive circulation based on this empirical result. The value of the other two vortex strengths is now determined by γ, which

is the only free parameter that we can use in an attempt to match our results to experiment. For Fig. 7.1(c) we have used $\gamma=\frac{1}{4}$, with the bottom vortex considered as vortex 2, i.e., the vortex strengths are taken to be in the proportion $\Gamma_1:\Gamma_2:\Gamma_3 = 3:1:(-4)$. Finally, the initial vortex positions are taken as those in the first triangle on the left in Fig. 7.1(b). We now integrate numerically in time through one full cycle of the cylinder oscillation, record the vortex locations, integrate through another cycle, again record the vortex locations, and so on to create the picture in Fig. 7.1(c). Note that we are using the doubly periodic solutions discussed previously – no attempt has been made to include image vortices in the cylinder, or to account for a wake flow of any kind.

It is difficult to claim too much for the comparison presented in Fig.7.1. However, we do believe that the following conclusions are merited: (1) The relative motion of three vortices shed during a cycle in the wake of an oscillating cylinder resemble the "unbounded" motions for the point vortex model problem in the sense that the "base vortices" separate ever more as the motion evolves, i.e., the downstream distance between vortices shed in the same cycle grows in time; the model problem explains the existence and likelihood of this type of motion. (2) The full solution of the model problem suggests that there are several other regimes of motion, counterparts of which have not so far been seen in the experiments; the model shows where in the (γ,X) parameter space one might expect to find these motions, but it cannot, of course, say anything about how to oscillate the cylinder in order to produce appropriate initial conditions for the vortices. (3) The full set of solutions to the point vortex problem clearly shows that the amount of mixing along the wake can be varied considerably depending on how the vortices are positioned immediately after one shedding cycle; this observation suggests that considerable control can be exercised over mixing in the wake of an oscillating cylinder by judicious choice of shedding frequency, amplitude and oscillation direction.

It would clearly be a very interesting and worthwhile step to establish additional correspondences between experimental parameters that govern three-vortex-per-cycle shedding patterns and the regimes of motion brought to light by the present analysis. Very sensitive dependence of wake evolution on shedding conditions may be observable close to conditions for which the ratio of two vortex strengths is an irrational number that is hard to approximate by rationals, such as the golden mean. However, the motion is always integrable regardless of the value of γ.

A preliminary report on this work was presented at the annual meeting of the APS Division of Fluid Dynamics in Atlanta, GA, November 1994 (Stremler & Aref, 1994). The support of NSF grant CTS–9311545 is gratefully acknowledged. MS also acknowledges the support of an ONR Fellowship.

References

Aref, H. 1979 Motion of three vortices. *Phys. Fluids* **22**, 393-400.

Aref, H. 1983 Integrable, chaotic, and turbulent vortex motion in two-dimensional flows. *Ann. Rev. Fluid Mech.* **15**, 345-389.

Aref, H. 1985 Chaos in the dynamics of a few vortices - fundamentals and applications. In *Theoretical and Applied Mechanics,* F. I. Niordson & N. Olhoff eds., North-Holland, Amsterdam, pp. 43-68.

Aref, H. 1989 Three-vortex motion with zero total circulation: Addendum. *J. Appl. Math. Phys. (ZAMP)* **40**, 495-500.

Aref, H., Rott, N. & Thomann, H. 1992 Gröbli's solution of the three-vortex problem. *Ann. Rev. Fluid Mech.* **24**, 1-20.

Birkhoff, G. & Fisher, J. 1959 Do vortex sheets roll up? *Rend. Circ. Mat. Palermo* **8**, 77-90.

Birkhoff, G. & Zarantonello, E. 1957 *Jets, Wakes and Cavities.* New York: Academic Press.

Blomberg, D. C. 1984 *Point Vortex Models of a Forced Shear Layer.* M. Sc. Thesis, Brown University.

Couder, Y. & Basdevant, C. 1986 Experimental and numerical study of vortex couples in two-dimensional flows. *J. Fluid Mech.* **173**, 225-251.

Eckhardt, B. 1989 Integrable four-vortex motion. *Phys. Fluids* **31**, 2796-2801.

Eckhardt, B. & Aref, H. 1988 Integrable and chaotic motions of four vortices II: Collision dynamics of vortex pairs. *Phil. Trans. Roy. Soc. (London) A* **326**, 655-696.

Griffin, O. M. & Ramberg, S. E. 1974 The vortex-street wakes of vibrating cylinders. *J. Fluid Mech.* **66**, 553-576.

Griffin, O. M. & Ramberg, S. E. 1976 Vortex shedding from a cylinder vibrating in line with an incident uniform flow. *J. Fluid Mech.* **75**, 257-271.

Griffin, O. M., Skop, R. A. & Koopman, G. H. 1973 The vortex-excited resonant vibrations of circular cylinders. *J. Sound Vibr.* **31**, 235-249.

Gröbli, W. 1877 *Specielle Probleme über die Bewegung geradliniger paralleler Wirbelfäden.* Zürich, Zürcher und Furrer, 86pp.

Honji, H. & Taneda, S. 1968 Vortex wakes of oscillating circular cylinders. *Rep. Res. Inst. Appl. Mech.* **16**, 211-222.

Kochin, N. E., Kibel, I. A. & Roze, N. V. 1964 *Theoretical Hydrodynamics.* Interscience.

Koopman, G. H. 1967 The vortex wakes of vibrating cylinders at low Reynolds numbers. *J. Fluid Mech.* **28**, 501-512.

Lamb, H. 1932 *Hydrodynamics.* 6th ed., Dover Publications, New York.

Novikov, E. A. 1975 Dynamics and statistics of a system of vortices. *Sov. Phys. JETP* **41**, 937-943.

Ongoren, A. & Rockwell, D. 1988 Flow structure from an oscillating cylinder II: Mode competition in the near wake. *J. Fluid Mech.* **191**, 225-245.

Rott, N. 1989 Three-vortex motion with zero total circulation. *J. Appl. Math. Phys. (ZAMP)* **40**, 473-494.

Rott, N. 1990 Constrained three- and four-vortex problems. *Phys. Fluids A* **2**, 1477-1480.

Rott, N. 1994 Four vortices on doubly periodic paths. *Phys. Fluids* **6**, 760-764.

Stremler, M. A. & Aref, H. 1994 Motion of three vortices in a periodic strip. *Bull. Amer. Phys. Soc.* **39**, 1890.

Synge, J. L. 1949 On the motion of three vortices. *Can. J. Math.* **1**, 257-270.

Williamson, C. H. K. & Roshko, A. 1988 Vortex formation in the wake of an oscillating cylinder. *J. Fluids Struct.* **2**, 355-381.

Figure Captions

Fig. 3.1: Phase space for $\Gamma_1:\Gamma_2:\Gamma_3 = 1:1:(-2)$, $\gamma=0$, and $X=0$. The strip width is 2L and there are two advecting vortices (solid dots). The four regimes of motion are labelled I-IV, the saddle points are A and B, and the separatrices are designated α, β, γ and δ.

Fig. 3.2: Real space trajectories of the three vortices corresponding to the phase space diagram of Fig.3.1. Base vortices are shown as solid circles, periodic images as open circles. Vortex 3 is stationary in all cases. Initial positions are labelled 1, 2; final positions 1', 2'. All motions are shown for one period (in the case of separatrices: for the transition from saddle to saddle). The motion in II, β, and δ is obtained by interchanging vortices 1 and 2 in I, α, and γ, respectively.

Fig. 3.3: Phase space for $\Gamma_1:\Gamma_2:\Gamma_3 = 1:1:(-2)$, $\gamma=0$, and a "generic" value of $X= (1 + i)/8$. The strip width is 2L and there are now four advecting vortices (solid dots). The regimes of motion are labelled I-VII, the saddle points are A-D, and the separatrices are designated by small Greek letters.

Fig. 3.4: Real space trajectories of the three vortices corresponding to the phase space diagram of Fig.3.3. Base vortices are shown as solid circles and their trajectories as heavier lines; periodic images are open circles and their trajectories are lighter lines. Initial positions are labelled 1, 2, 3; final positions 1', 2', 3'. Final positions of required periodic images are labelled 1", 2", 3". The trajectories are labelled according to the regimes and separatrices indicated in Fig.3.3. All motions are shown for one period (in the case of separatrices: for the transition from saddle to saddle). Note that since vortices 1 and 2 may be interchanged, regimes and separatrices pairwise may lead to similar real space trajectories. The motion in II, β, δ, φ, and θ is obtained by interchanging vortices 1 and 2 in I, α, γ, ε, and ν, respectively.

Fig. 5.1: Phase space for $\Gamma_1:\Gamma_2:\Gamma_3 = 2:1:(-3)$, $\gamma=1/6$, and a "generic" value of $X= (1+3i)/12$. The strip width is 3L and there are 6 advecting vortices (solid dots). The regimes of motion are labelled I-XIII, the saddle points are A-F, and the separatrices are designated by small Greek letters. Note the lack of connection between saddle points such as D and E that "belong" to the same "dipole-like" structure. Note also the very thin regimes of motion, such as IX, XI and XII.

Fig. 5.2: Phase space for the same set of vortices as in Fig.5.1, $\Gamma_1:\Gamma_2:\Gamma_3 = 2:1:(-3)$, $\gamma=1/6$, but for special values of X, (a) i/4; (b) (2+3i)/12. For these values certain symmetries arise which lead to various saddle points being connected, and thus to fewer regimes of motion. The strip width is 3L and there are 6 advecting vortices (solid dots). The regimes of motion and the separatrices have not been labelled in order to highlight the simpler topology of the diagrams compared to the "generic" case in Fig.5.1.

Fig. 5.3: Real space trajectories of the three vortices corresponding to the phase space diagram of Fig.5.1. Base vortices are shown as solid circles and their trajectories as heavier lines; periodic images are open circles and their trajectories are lighter lines. The trajectories are labelled according to the regimes indicated in Fig.5.1. Initial positions are labelled 1, 2, 3; final positions 1', 2', 3'. Final positions of required periodic images are labelled 1", 2", 3". All motions are shown for one period.

Fig. 5.4: Real space trajectories of the three vortices corresponding to the phase space diagram of Fig.5.1. Base vortices are shown as solid circles and their trajectories as heavier lines; periodic images are open circles and their trajectories are lighter lines. These trajectories correspond and are labelled according to the separatrices indicated in Fig.5.1. Initial positions are labelled 1, 2, 3; final positions 1', 2', 3'. Final positions of required periodic images are labelled 1", 2", 3". All motions are shown for the transition from saddle to saddle.

Fig. 5.5: Phase space for $\Gamma_1:\Gamma_2:\Gamma_3 = 7:3:(-10)$, $\gamma=1/5$, and $X = (3+10i)/40$. The strip width is 10L and there are 20 advecting vortices (solid dots). Two separatrices are labelled (cf. Fig. 5.6).

Fig. 5.6: Real space trajectories of the three vortices corresponding to the two separatrices α and β in the phase space diagram of Fig.5.5. Base vortices are shown as solid circles and their trajectories as heavier lines; periodic images are open circles and their trajectories are lighter lines. Initial positions are labelled 1, 2, 3; final positions 1', 2', 3'. Final positions of required periodic images are labelled 1", 2", 3". All motions are shown for the transition from saddle to saddle.

Fig. 5.7: Phase space for $\Gamma_1:\Gamma_2:\Gamma_3 = 9:1:(-10)$, $\gamma=2/5$, and $X = (1+10i)/40$. The strip width is 10L and there are 20 advecting vortices (solid dots). Three separatrices are labelled (cf. Fig. 5.8).

Fig. 5.8: Real space trajectories of the three vortices corresponding to the three separatrices α, β and γ in the phase space diagram of Fig.5.7. Base vortices are shown as solid circles and their trajectories as heavier lines; periodic images are open circles and their trajectories are lighter lines. Initial positions are labelled 1, 2, 3; final positions 1', 2', 3'. Final positions of required periodic images are labelled 1", 2", 3". All motions are shown for the transition from saddle to saddle.

Fig. 7.1: Comparison of flow visualization of the wake of an oscillating cylinder (Roshko & Williamson 1988) and point vortex model solutions.

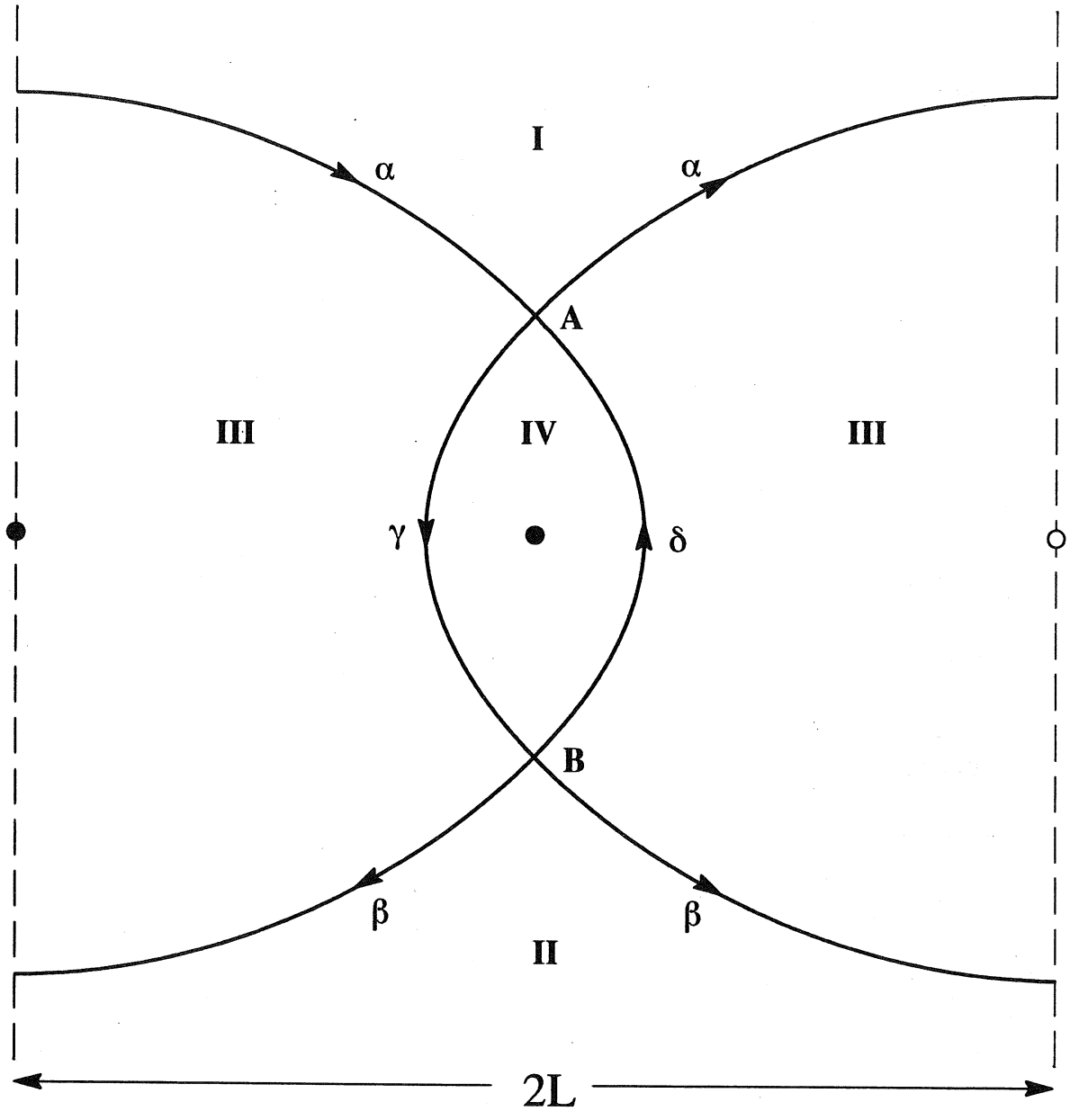

Fig. 3.1

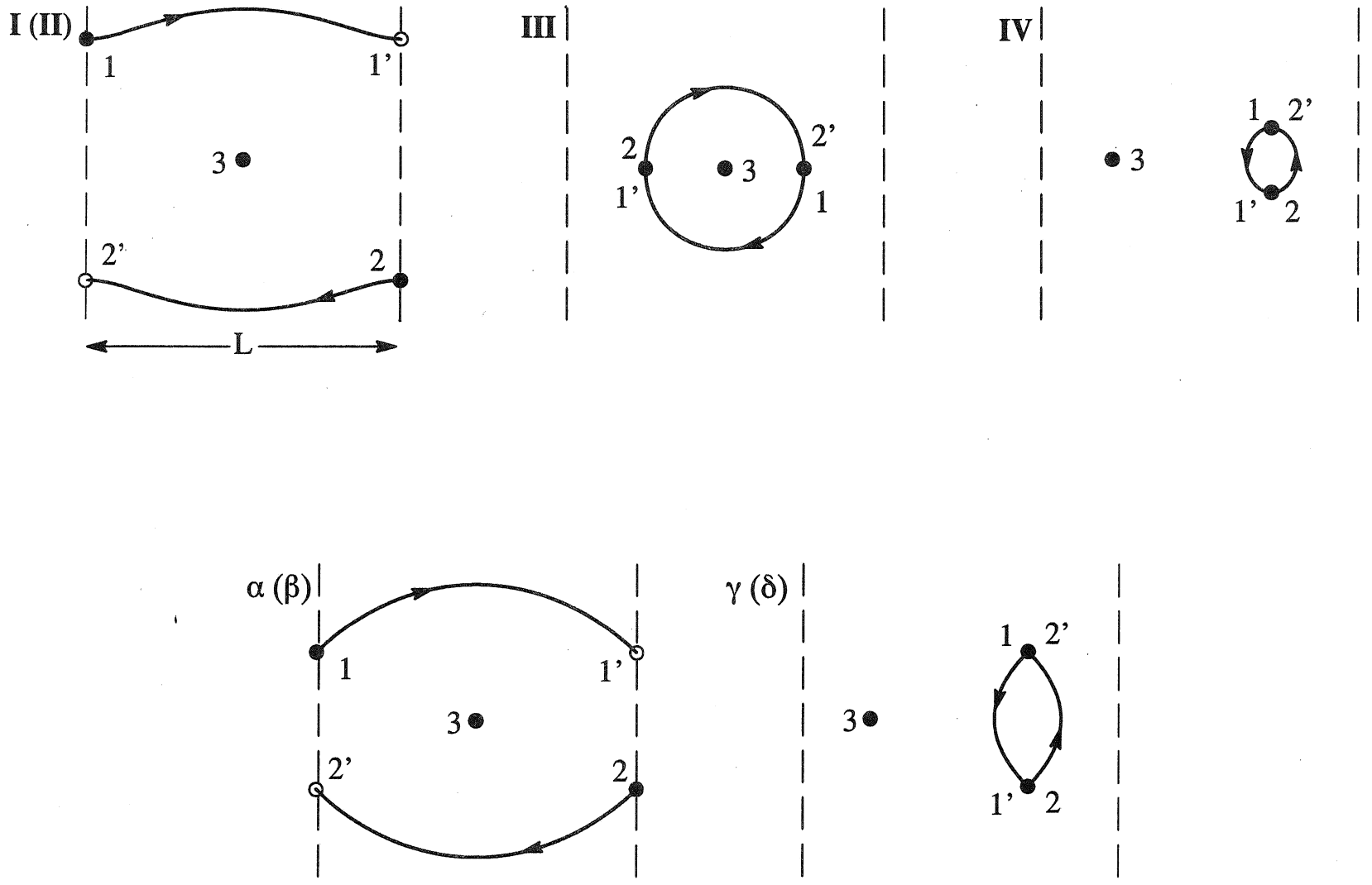

Fig. 3.2

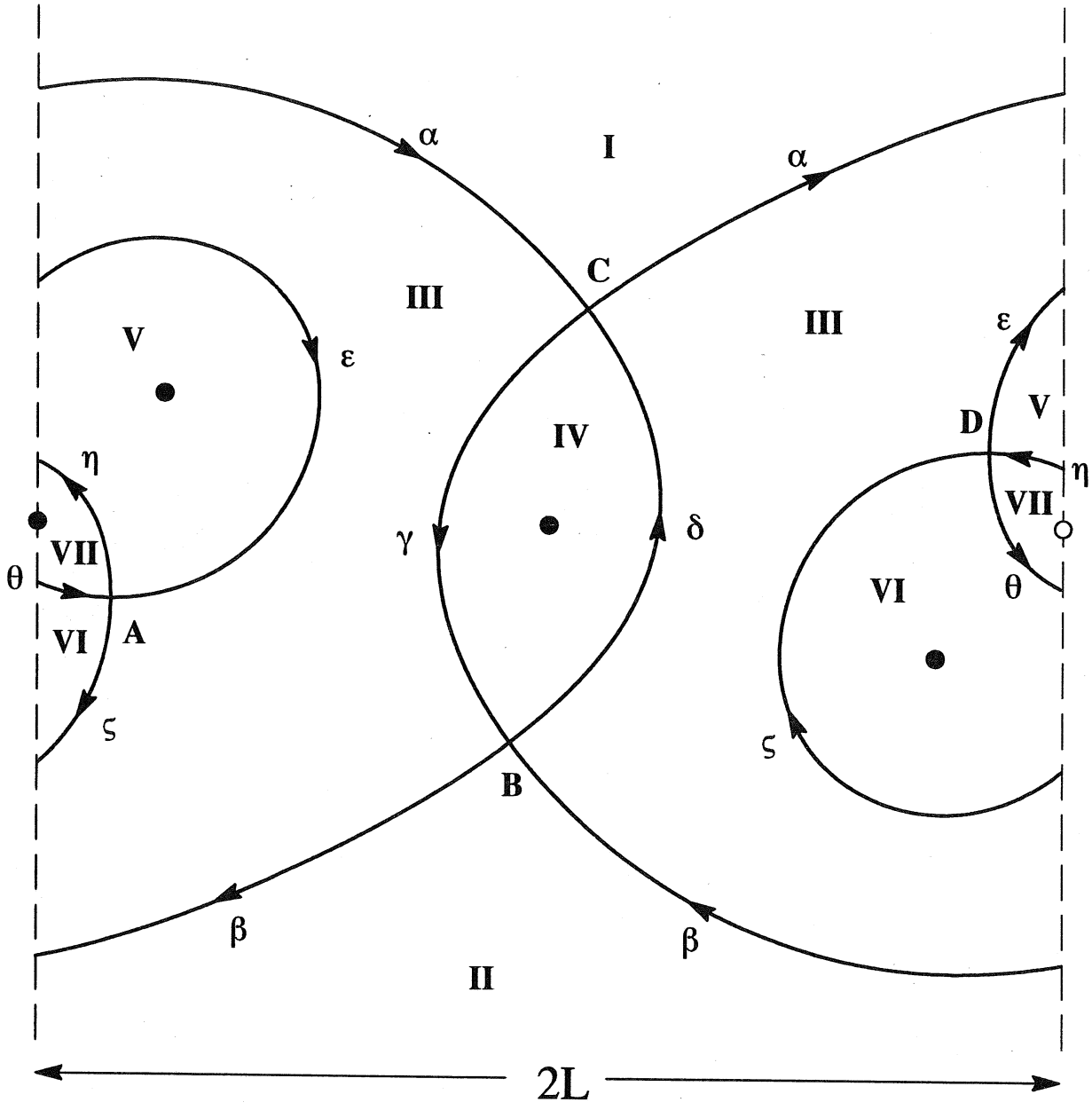

Fig. 3.3

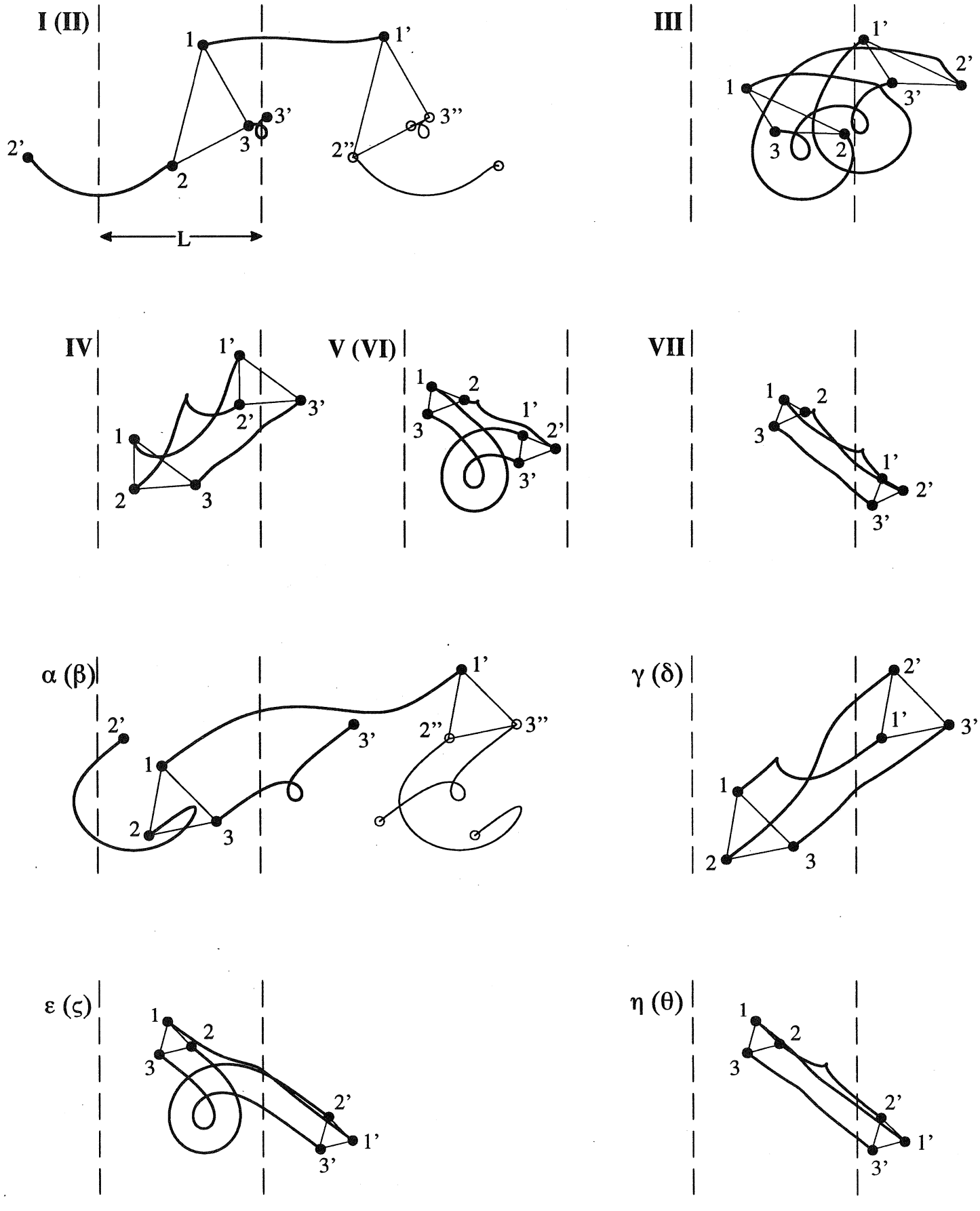
I (II)
1
1'
2'
2
3
3'
2''
3''
L
III
1'
2'
1
3'
3
2
IV
1'
3'
2'
1
2
3
V (VI)
1
2
1'
3
2'
3'
VII
1
2
3
1'
2'
3'
α (β)
1'
2'
3'
2''
3''
1
2
3
γ (δ)
2'
1'
3'
1
2
3
ε (ς)
1
2
3
2'
1'
3'
η (θ)
1
2
3
2'
1'
3'

Fig. 3.4

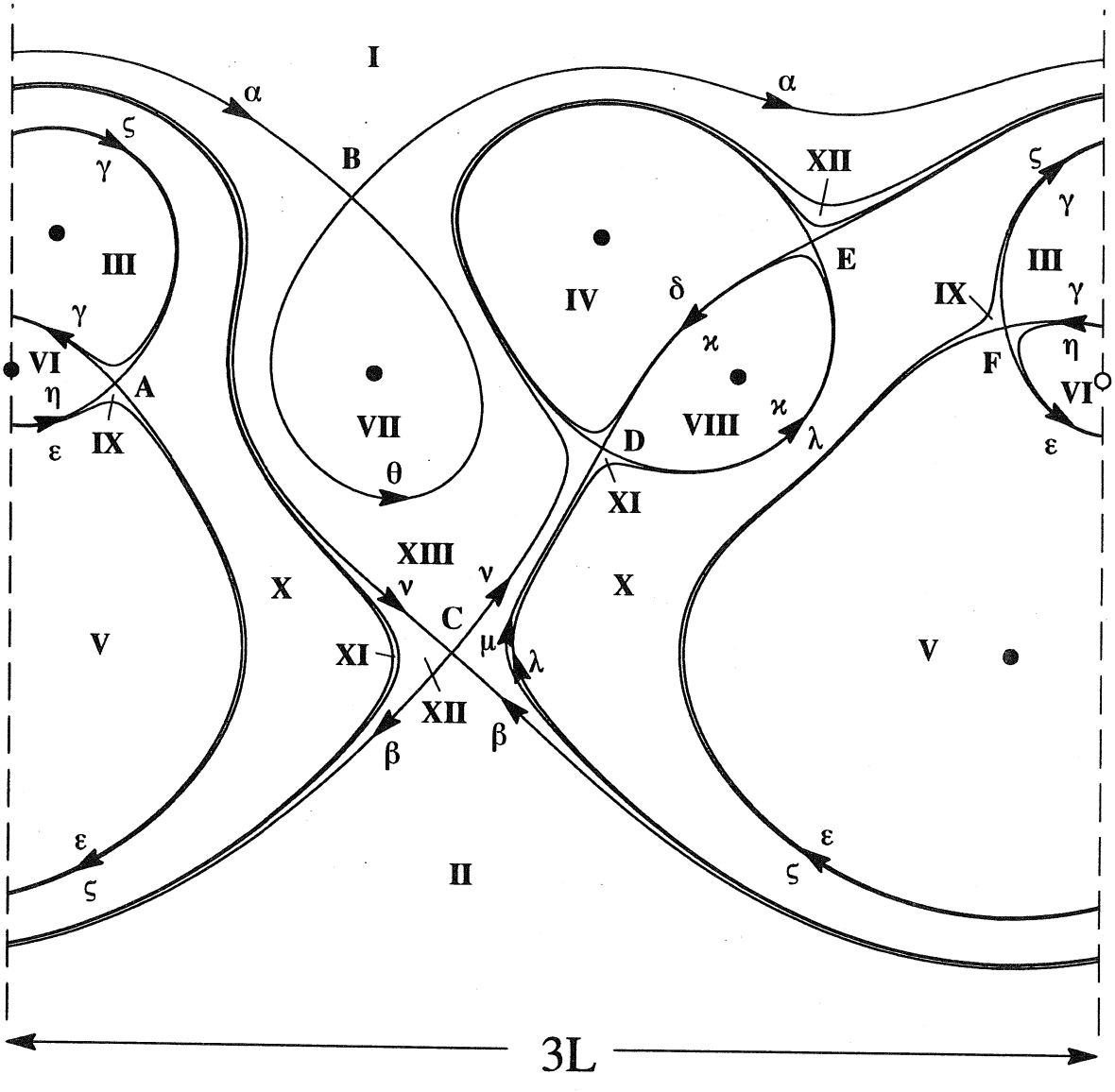
I
α
ς
γ
B
III
γ
VI
η
A
ε
IX
VII
θ
XIII
ν
X
V
C
XI
μ
λ
XII
β
ε
ς
II
α
XII
ς
γ
E
δ
IV
III
IX
γ
κ
η
F
VI
D
VIII
κ
λ
ε
XI
X
V
ε
ς
3L

Fig. 5.1

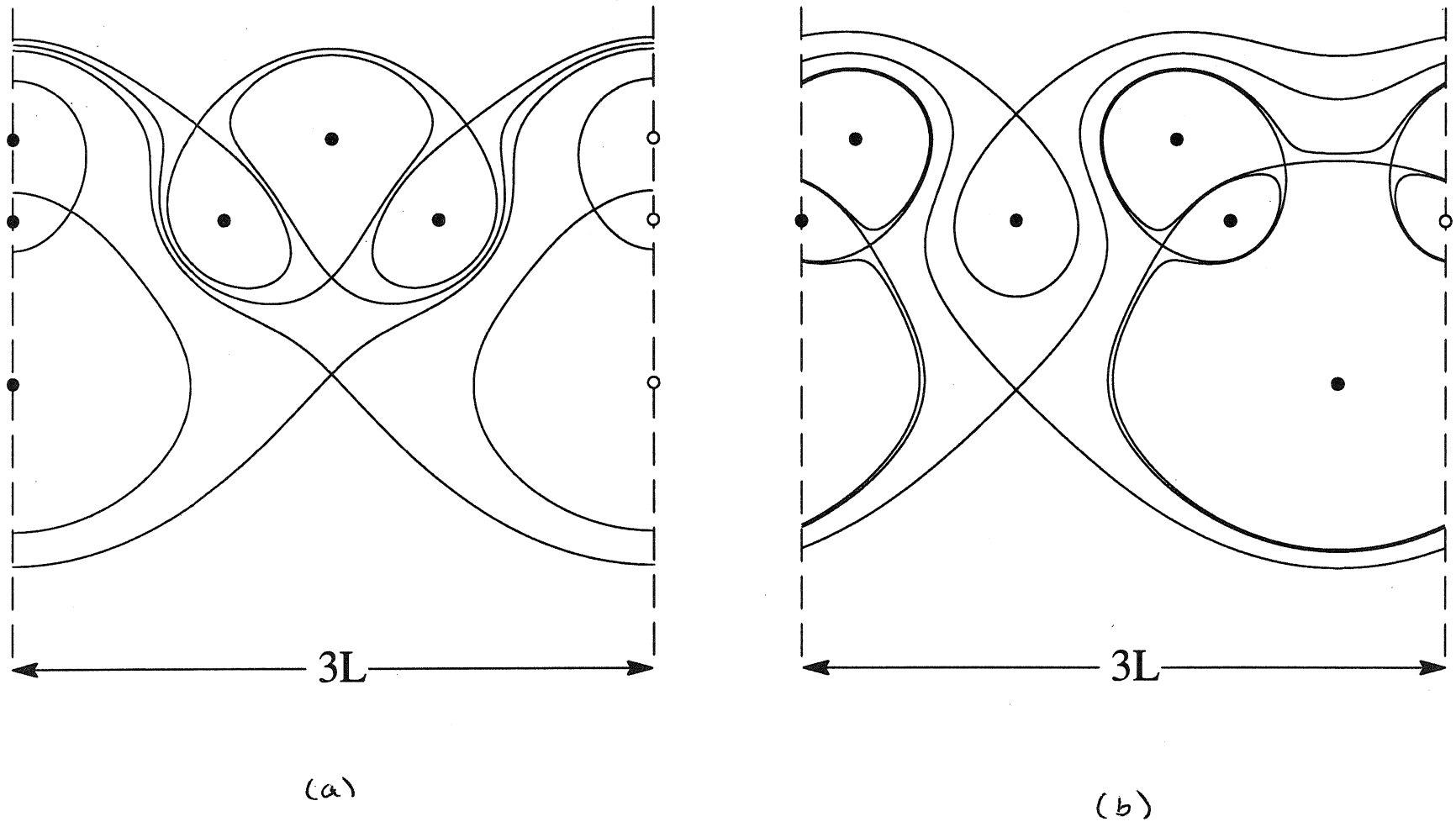

Fig. 5.2

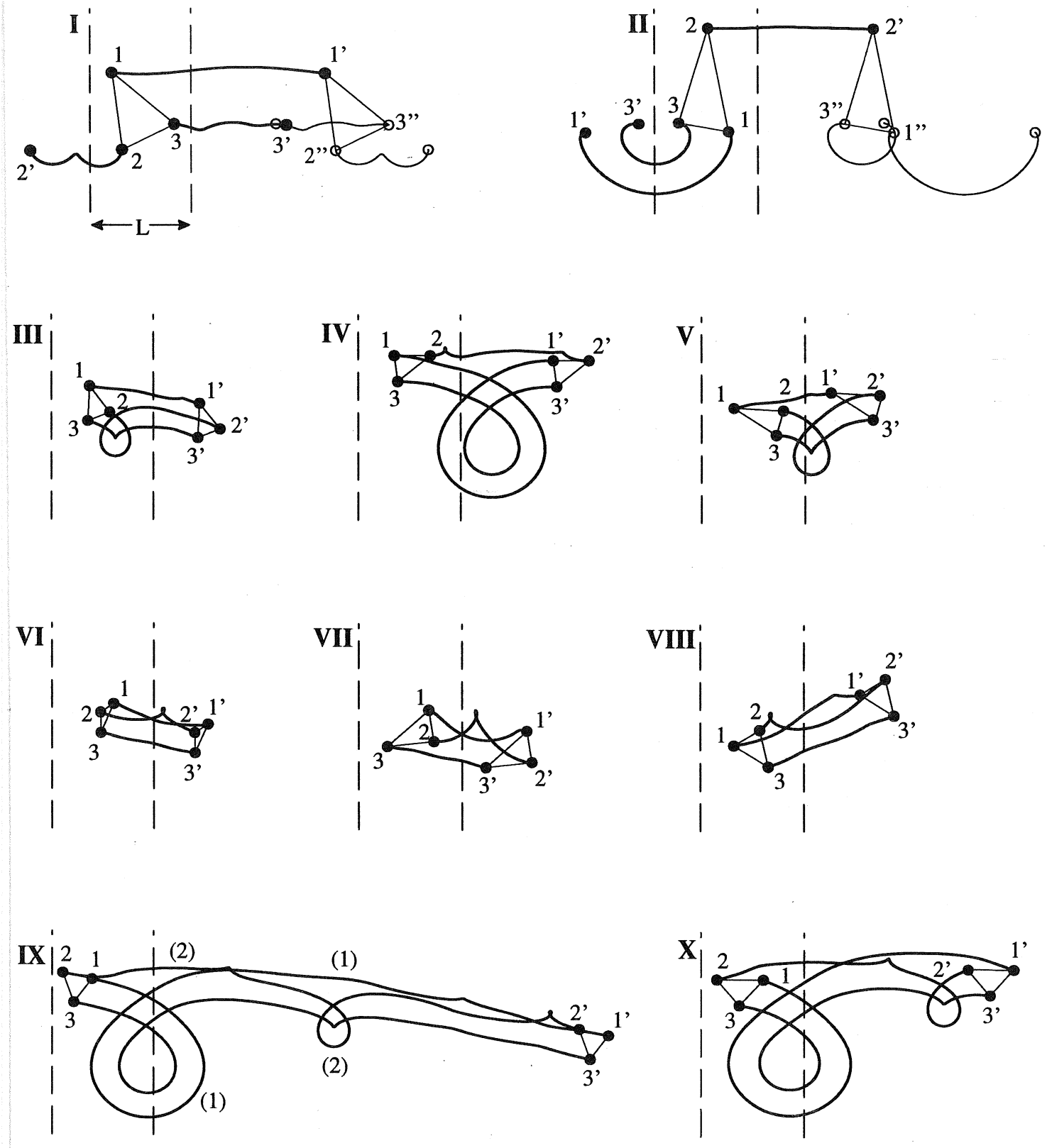
I
1
1'
3"
3
3'
2"
2'
2
L
II
2
2'
1'
3'
3
1
3"
1"
III
1
1'
2
3
2'
3'
IV
1
2
1'
2'
3
3'
V
1
2
1'
2'
3
3'
VI
1
2
2'
1'
3
3'
VII
1
2
1'
3
3'
2'
VIII
2'
1'
2
1
3'
3
IX
2
1
(2)
(1)
3
2'
1'
(2)
3'
(1)
X
2
1
1'
2'
3
3'

Fig. 5.3

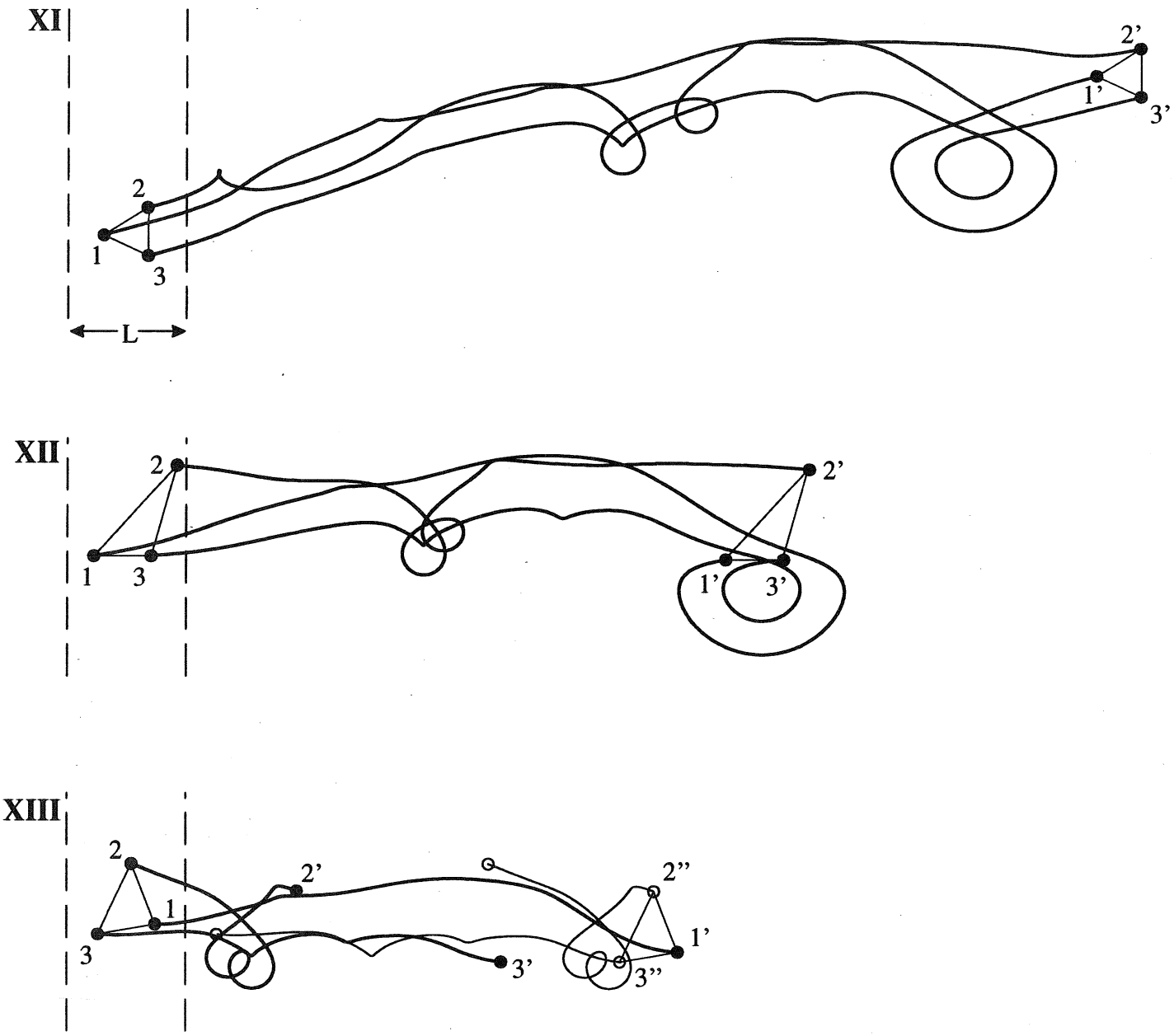

Fig. 5.3 (cont)

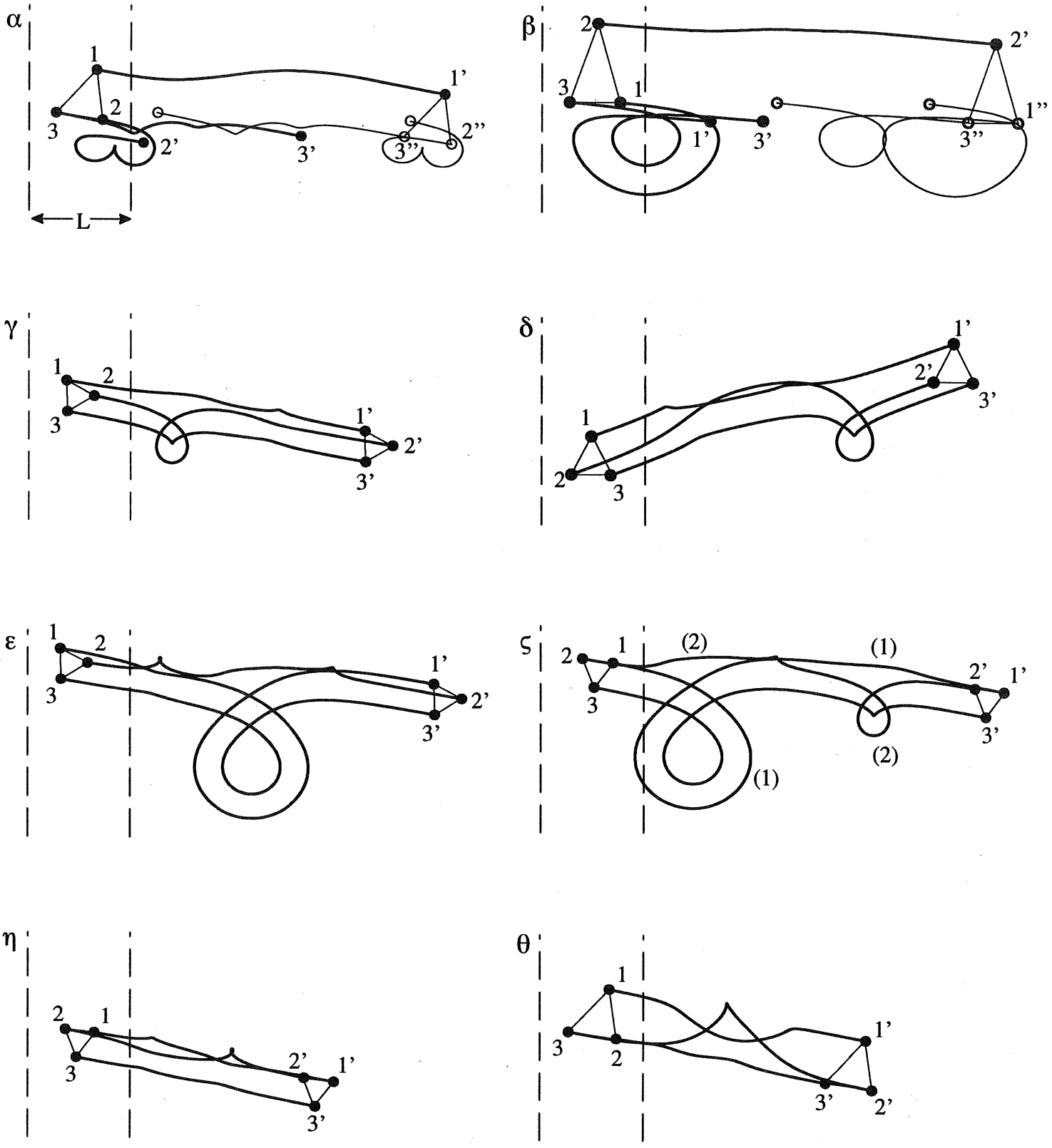
α
1
2
3
1'
2'
3'
2"
3"
L
β
2
3
1
2'
1'
3'
1"
3"
γ
1
2
3
1'
2'
3'
δ
1'
2'
3'
1
2
3
ε
1
2
3
1'
2'
3'
ς
2
1
(2)
(1)
3
2'
1'
3'
(2)
(1)
η
2
1
3
2'
1'
3'
θ
1
3
2
1'
3'
2'

Fig. 5.4

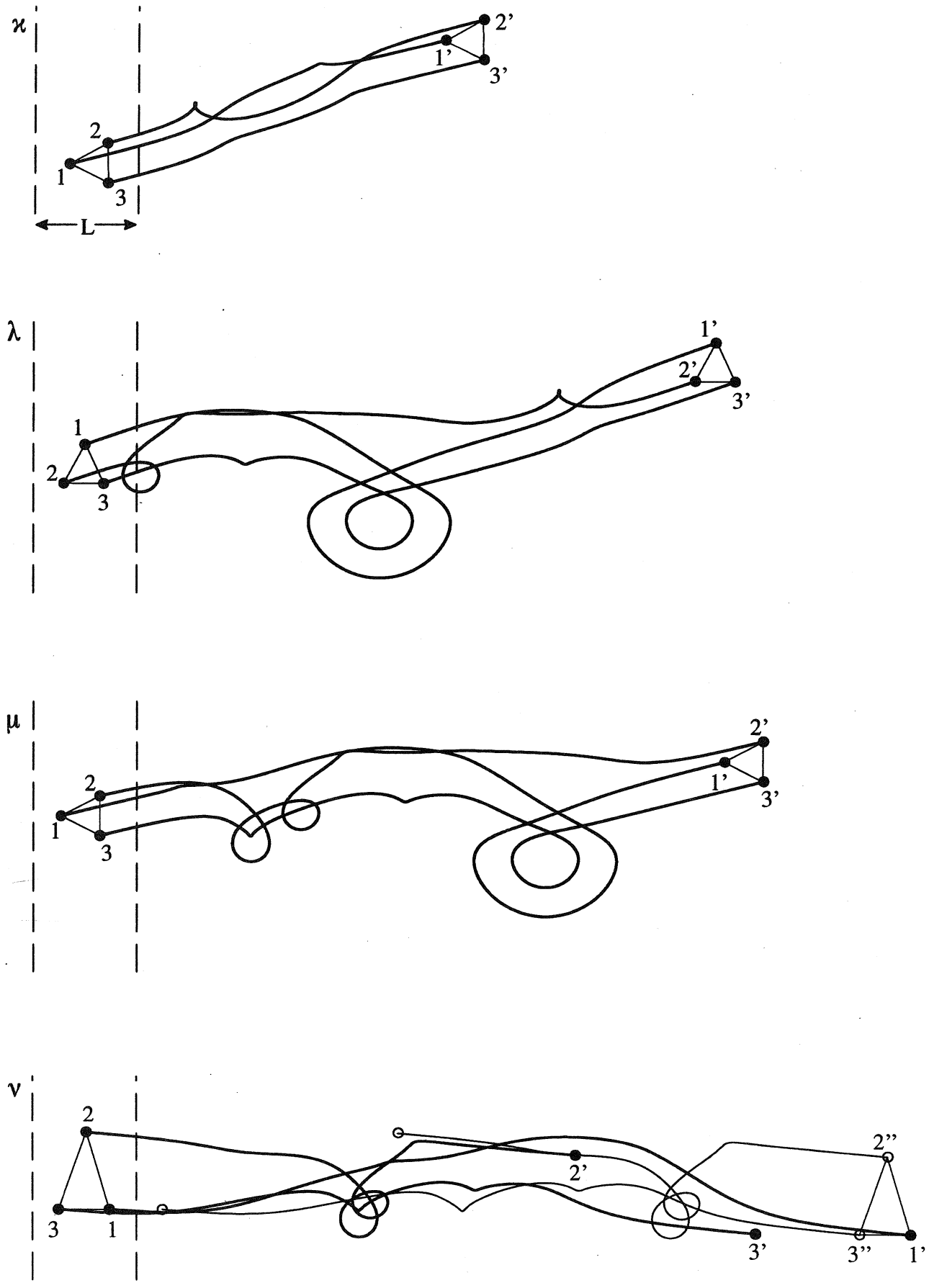

Fig. 5.4 (cont.)

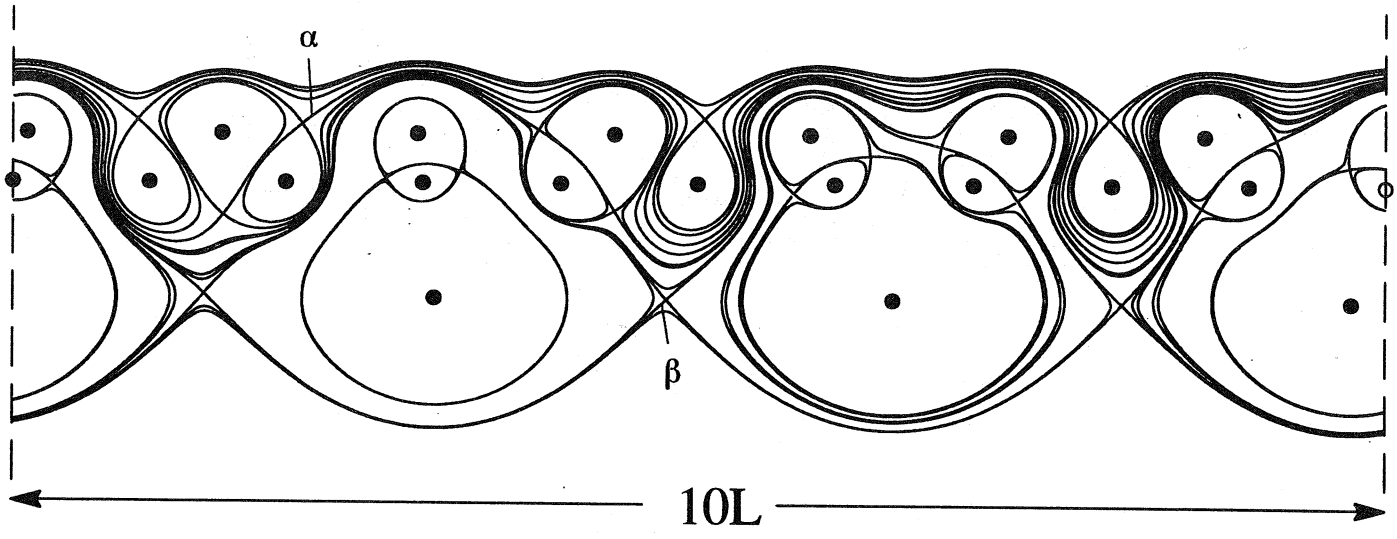

Fig. 5.5

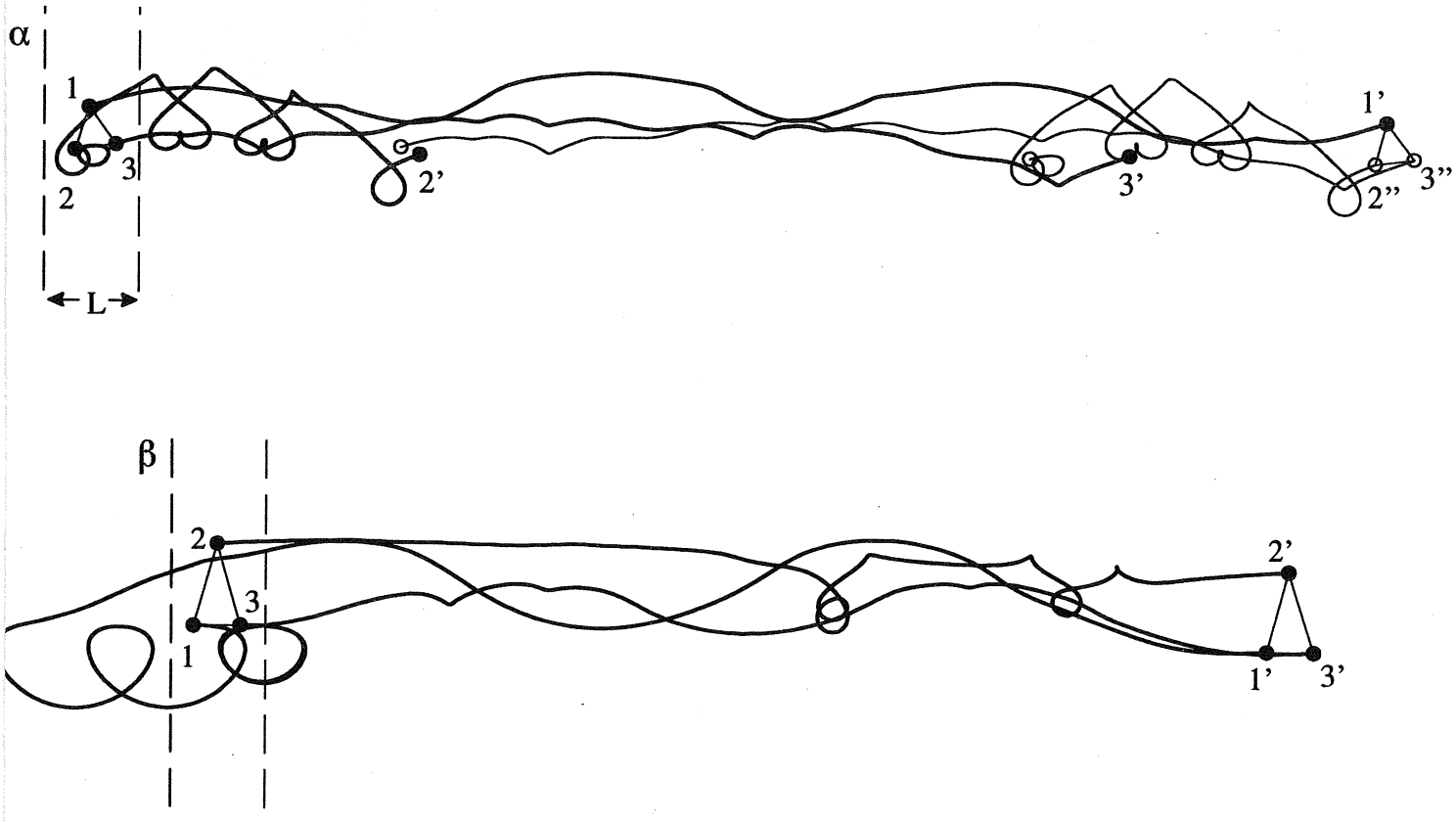

Fig. 5.6

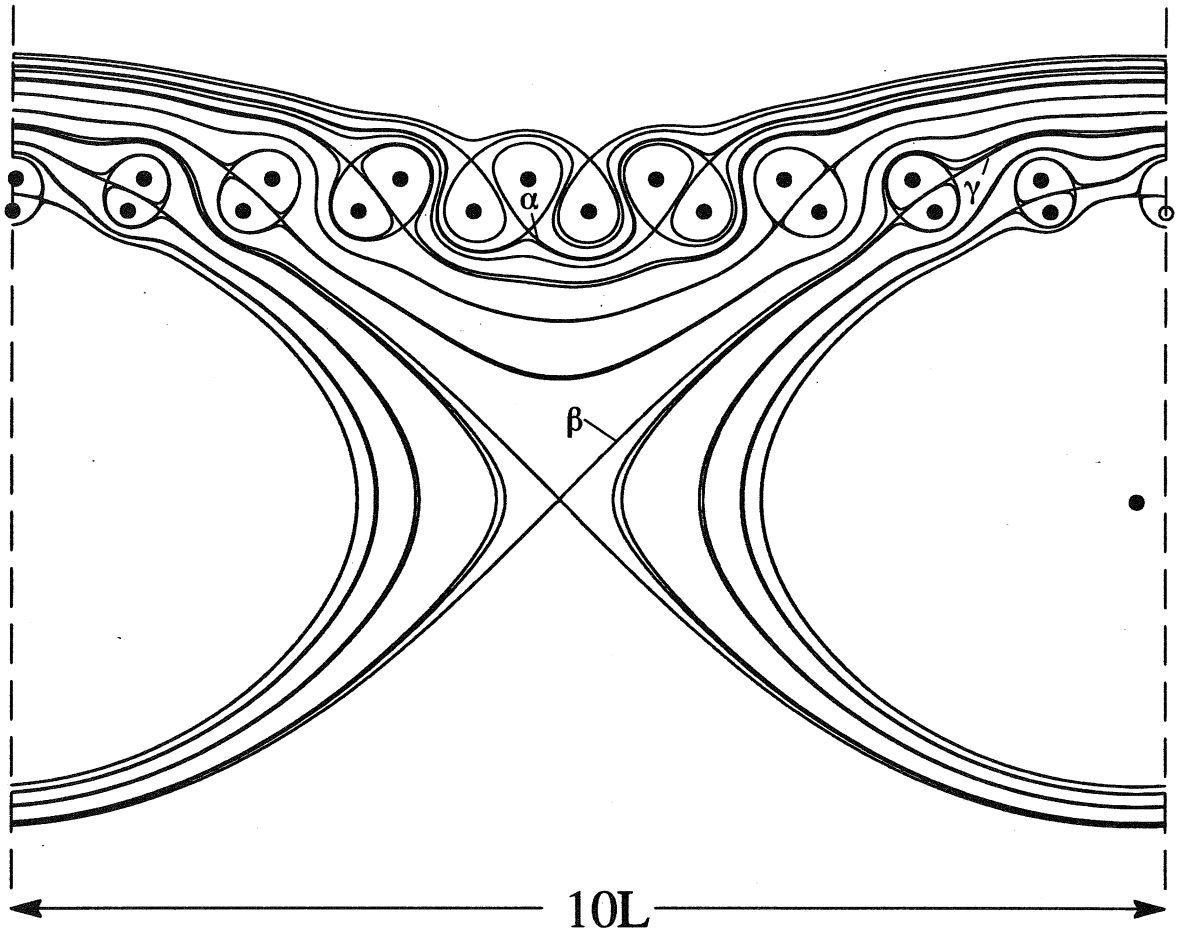

Fig. 5.7

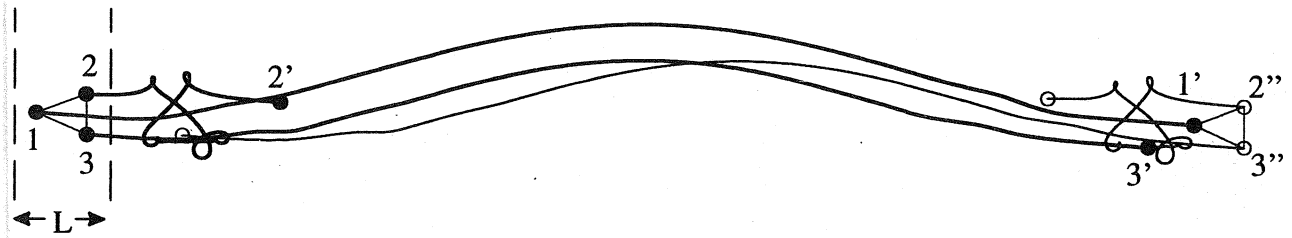

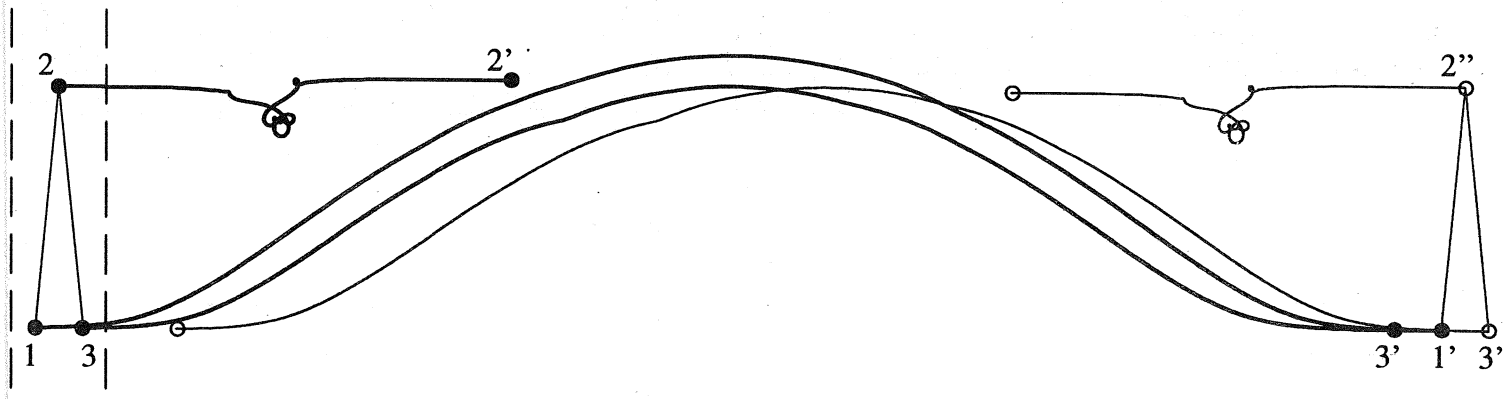

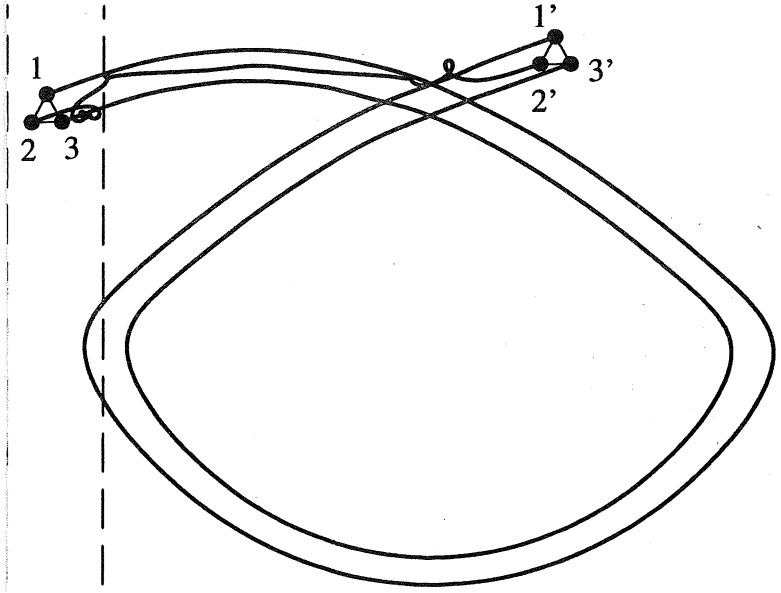

Fig. 5.8

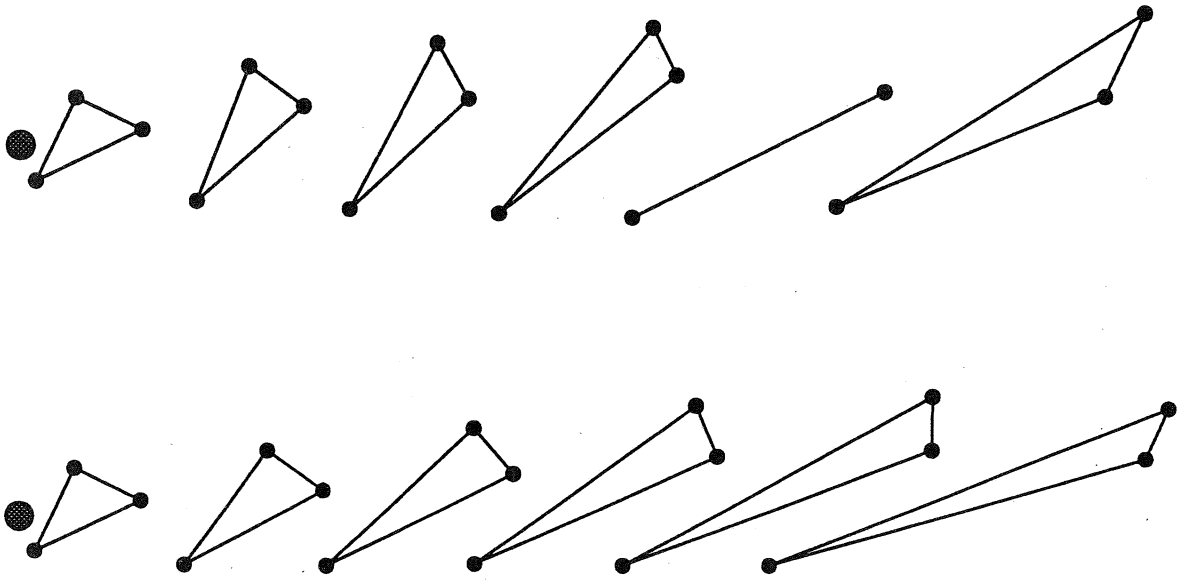

Fig. 7.1

List of Recent TAM Reports

No.	*Authors*	*Title*	*Date*
714	Birnbaum, H. K., and P. Sofronis	Hydrogen-enhanced localized plasticity—A mechanism for hydrogen-related fracture	July 1993
715	Balachandar, S., and M. R. Malik	Inviscid instability of streamwise corner flow	July 1993
716	Sofronis, P.	Linearlized hydrogen elasticity	July 1993
717	Nitzsche, V. R., and K. J. Hsia	Modelling of dislocation mobility controlled brittle-to-ductile transition	July 1993
718	Hsia, K. J., and A. S. Argon	Experimental study of the mechanisms of brittle-to-ductile transition of cleavage fracture in silicon single crystals	July 1993
719	Cherukuri, H. P., and T. G. Shawki	An energy-based localization theory: Part II—Effects of the diffusion, inertia and dissipation numbers	Aug. 1993
720	Aref, H., and S. W. Jones	Chaotic motion of a solid through ideal fluid	Aug. 1993
721	Stewart, D. S.	Lectures on detonation physics: Introduction to the theory of detonation shock dynamics	Aug. 1993
722	Lawrence, C. J., and R. Mei	Long-time behavior of the drag on a body in impulsive motion	Sept. 1993
723	Mei, R., J. F. Klausner, and C. J. Lawrence	A note on the history force on a spherical bubble at finite Reynolds number	Sept. 1993
724	Qi, Q., R. E. Johnson, and J. G. Harris	A re-examination of the boundary layer attenuation and acoustic streaming accompanying plane wave propagation in a circular tube	Sept. 1993
725	Turner, J. A., and R. L. Weaver	Radiative transfer of ultrasound	Sept. 1993
726	Yogeswaren, E. K., and J. G. Harris	A model of a confocal ultrasonic inspection system for interfaces	Sept. 1993
727	Yao, J., and D. S. Stewart	On the normal detonation shock velocity–curvature relationship for materials with large activation energy	Sept. 1993
728	Qi, Q.	Attenuated leaky Rayleigh waves	Oct. 1993
729	Sofronis, P., and H. K. Birnbaum	Mechanics of hydrogen–dislocation–impurity interactions: Part I—Increasing shear modulus	Oct. 1993
730	Hsia, K. J., Z. Suo, and W. Yang	Cleavage due to dislocation confinement in layered materials	Oct. 1993
731	Acharya, A., and T. G. Shawki	A second-deformation-gradient theory of plasticity	Oct. 1993
732	Michaleris, P., D. A. Tortorelli, and C. A. Vidal	Tangent operators and design sensitivity formulations for transient nonlinear coupled problems with applications to elasto-plasticity	Nov. 1993
733	Michaleris, P., D. A. Tortorelli, and C. A. Vidal	Analysis and optimization of weakly coupled thermo-elasto-plastic systems with applications to weldment design	Nov. 1993
734	Ford, D. K., and D. S. Stewart	Probabilistic modeling of propellant beds exposed to strong stimulus	Nov. 1993
735	Mei, R., R. J. Adrian, and T. J. Hanratty	Particle dispersion in isotropic turbulence under the influence of non-Stokesian drag and gravitational settling	Nov. 1993
736	Dey, N., D. F. Socie, and K. J. Hsia	Static and cyclic fatigue failure at high temperature in ceramics containing grain boundary viscous phase: Part I—Experiments	Nov. 1993
737	Dey, N., D. F. Socie, and K. J. Hsia	Static and cyclic fatigue failure at high temperature in ceramics containing grain boundary viscous phase: Part II—Modelling	Nov. 1993
738	Turner, J. A., and R. L. Weaver	Radiative transfer and multiple scattering of diffuse ultrasound in polycrystalline media	Nov. 1993
739	Qi, Q., and R. E. Johnson	Resin flows through a porous fiber collection in pultrusion processing	Dec. 1993

List of Recent TAM Reports (cont'd)

No.	*Authors*	*Title*	*Date*
740	Weaver, R. L., W. Sachse, and K. Y. Kim	Transient elastic waves in a transversely isotropic plate	Dec. 1993
741	Zhang, Y., and R. L. Weaver	Scattering from a thin random fluid layer	Dec. 1993
742	Weaver, R. L., and W. Sachse	Diffusion of ultrasound in a glass bead slurry	Dec. 1993
743	Sundermeyer, J. N., and R. L. Weaver	On crack identification and characterization in a beam by nonlinear vibration analysis	Dec. 1993
744	Li, L., and N. R. Sottos	Predictions of static displacements in 1–3 piezocomposites	Dec. 1993
745	Jones, S. W.	Chaotic advection and dispersion	Jan. 1994
746	Stewart, D. S., and J. Yao	Critical detonation shock curvature and failure dynamics: Developments in the theory of detonation shock dynamics	Feb. 1994
747	Mei, R., and R. J. Adrian	Effect of Reynolds-number-dependent turbulence structure on the dispersion of fluid and particles	Feb. 1994
748	Liu, Z.-C., R. J. Adrian, and T. J. Hanratty	Reynolds-number similarity of orthogonal decomposition of the outer layer of turbulent wall flow	Feb. 1994
749	Barnhart, D. H., R. J. Adrian, and G. C. Papen	Phase-conjugate holographic system for high-resolution particle image velocimetry	Feb. 1994
750	Qi, Q., W. D. O'Brien Jr., and J. G. Harris	The propagation of ultrasonic waves through a bubbly liquid into tissue: A linear analysis	March 1994
751	Mittal, R., and S. Balachandar	Direct numerical simulation of flow past elliptic cylinders	May 1994
752	Anderson, D. N., J. R. Dahlen, M. J. Danyluk, A. M. Dreyer, K. M. Durkin, J. J. Kriegsmann, J. T. McGonigle, and V. Tyagi	Thirty-first student symposium on engineering mechanics, J. W. Phillips, coord.	May 1994
753	Thoroddsen, S. T.	The failure of the Kolmogorov refined similarity hypothesis in fluid turbulence	May 1994
754	Turner, J. A., and R. L. Weaver	Time dependence of multiply scattered diffuse ultrasound in polycrystalline media	June 1994
755	Riahi, D. N.	Finite-amplitude thermal convection with spatially modulated boundary temperatures	June 1994
756	Riahi, D. N.	Renormalization group analysis for stratified turbulence	June 1994
757	Riahi, D. N.	Wave-packet convection in a porous layer with boundary imperfections	June 1994
758	Jog, C. S., and R. B. Haber	Stability of finite element models for distributed-parameter optimization and topology design	July 1994
759	Qi, Q., and G. J. Brereton	Mechanisms of removal of micron-sized particles by high-frequency ultrasonic waves	July 1994
760	Shawki, T. G.	On shear flow localization with traction-controlled boundaries	July 1994
761	Balachandar, S., D. A. Yuen, and D. M. Reuteler	High Rayleigh number convection at infinite Prandtl number with temperature-dependent viscosity	July 1994
762	Phillips, J. W.	Arthur Newell Talbot—Proceedings of a conference to honor TAM's first department head and his family	Aug. 1994
763	Man., C. S., and D. E. Carlson	On the traction problem of dead loading in linear elasticity with initial stress	Aug. 1994
764	Zhang, Y., and R. L. Weaver	Leaky Rayleigh wave scattering from elastic media with random microstructures	Aug. 1994
765	Cortese, T. A., and S. Balachandar	High-performance spectral simulation of turbulent flows in massively parallel machines with distributed memory	Aug. 1994

List of Recent TAM Reports (cont'd)

No.	*Authors*	*Title*	*Date*
766	Balachandar, S.	Signature of the transition zone in the tomographic results extracted through the eigenfunctions of the two-point correlation	Sept. 1994
767	Piomelli, U.	Large-eddy simulation of turbulent flows	Sept. 1994
768	Harris, J. G., D. A. Rebinsky, and G. R. Wickham	An integrated model of scattering from an imperfect interface	Sept. 1994
769	Hsia, K. J., and Z. Xu	The mathematical framework and an approximate solution of surface crack propagation under hydraulic pressure loading	Sept. 1994
770	Balachandar, S.	Two-point correlation and its eigen-decomposition for optimal characterization of mantle convection	Oct. 1994
771	Lufrano, J. M., and P. Sofronis	Numerical analysis of the interaction of solute hydrogen atoms with the stress field of a crack	Oct. 1994
772	Aref, H., and S. W. Jones	Motion of a solid body through ideal fluid	Oct. 1994
773	Stewart, D. S., T. Aslam, J. Yao, and J. B. Bdzil	Level-set techniques applied to unsteady detonation propagation	Oct. 1994
774	Mittal, R., and S. Balachandar	Effect of three-dimensionality on the lift and drag of circular and elliptic cylinders	Oct. 1994
775	Stewart, D. S., T. D. Aslam, and J. Yao	The evolution of detonation cells	Nov. 1994
776	Aref, H.	On the equilibrium and stability of a row of point vortices	Nov. 1994
777	Cherukuri, H. P., T. G. Shawki, and M. El-Raheb	An accurate finite-difference scheme for elastic wave propagation in a circular disk	Nov. 1994
778	Li, L., and N. R. Sottos	Improving hydrostatic performance of 1–3 piezocomposites	Dec. 1994
779	Phillips, J. W., D. L. de Camara, M. D. Lockwood, and W. C. C. Grebner	Strength of silicone breast implants	Jan. 1995
780	Xin, Y.-B., K. J. Hsia, and D. A. Lange	Quantitative characterization of the fracture surface of silicon single crystals by confocal microscopy	Jan. 1995
781	Yao, J., and D. S. Stewart	On the dynamics of multi-dimensional detonation	Jan. 1995
782	Riahi, D. N., and T. L. Sayre	Effect of rotation on the structure of a convecting mushy layer	Feb. 1995
783	Batchelor, G. K., and TAM faculty and students	A conversation with Professor George K. Batchelor	Feb. 1995
784	Sayre, T. L., and D. N. Riahi	Effect of rotation on flow instabilities during solidification of a binary alloy	Feb. 1995
785	Xin, Y.-B., and K. J. Hsia	A technique to generate straight surface cracks for studying the dislocation nucleation condition in brittle materials	March 1995
786	Riahi, D. N.	Finite bandwidth, long wavelengh convection with boundary imperfections: Near-resonant wavelengh excitation	March 1995
787	Turner, J. A., and R. L. Weaver	Average response of an infinite plate on a random foundation	March 1995
788	Weaver, R. L., and D. Sornette	The range of spectral correlations in pseudointegrable systems: GOE statistics in a rectangular membrane with a point scatterer	April 1995

List of Recent TAM Reports (cont'd)

No.	*Authors*	*Title*	*Date*
789	Anderson, K. F., M. B. Bishop, B. C. Case, S. R. McFarlin, J. M. Nowakowski, D. W. Peterson, C. V. Robertson, and C. E. Tsoukatos	Thirty-second student symposium on engineering mechanics, J. W. Phillips, coord.	April 1995
790	Figa, J., and C. J. Lawrence	Linear stability analysis of a gravity-driven Newtonian coating flow on a planar incline	May 1995
791	Figa, J., and C. J. Lawrence	Linear stability analysis of a gravity-driven viscosity-stratified Newtonian coating flow on a planar incline	May 1995
792	Cherukuri, H. P., and T. G. Shawki	On shear band nucleation and the finite propagation speed of thermal disturbances	May 1995
793	Harris, J. G.	Modeling scanned acoustic imaging of defects at solid interfaces	May 1995
794	Sottos, N. R., J. M. Ockers, and M. J. Swindeman	Thermoelastic properties of plain weave composites for multilayer circuit board applications	May 1995
795	Aref, H., and M. A. Stremler	On the motion of three point vortices in a periodic strip	June 1995